Mixed host co-assembled systems for broad-scope analyte sensing

Allison J. Selinger,[1,2‡] Joana Krämer,[1,2,3‡] Eric Poarch,[4] Dennis Hore,[1,4] Frank Biedermann,[3*] Fraser Hof[1,2*]

[1]Department of Chemistry, University of Victoria, Victoria, BC V8P 5C2 Canada

[2]Centre for Advanced Materials and Related Technology (CAMTEC), University of Victoria, Victoria, BC V8W 2Y2, Canada

[3]Institute of Nanotechnology (INT), Karlsruhe Institute of Technology (KIT), Kaiserstraße 12, 76131 Karlsruhe, Germany

[4]Canadian Institute for Substance Use Research, University of Victoria, Victoria, BC V8W 2Y2, Canada

ABSTRACT: Here we report a systems-oriented approach to developing information-rich mixed host chemosensors. We show that co-assembling macrocyclic hosts from different classes, DimerDye sulfonatocalix[4]arenes and cucurbit[*n*]urils, effectively increases the scope of analyte binding interactions and therefore, sensory outputs. This simple dynamic strategy exploits cross-reactive noncovalent host-host complexation interactions while integrating a reporter dye, thereby producing emergent photophysical responses when an analyte interacts with either host. We first demonstrate the advantages of mixed host co-assembled chemosensors through an increased detection range of hydrophobic, cationic, neutral, and anionic drugs. We then implement mixed host sensors in an array-based platform for the differentiation of illicit drugs, including cannabinoids, benzodiazepine analogs, opiates, anesthetics, amphetamine, and common adulterating substances. Finally, the potential of this approach is applied to profiling real-world multi-component illicit street drug samples, proving to be more effective than classical sensor arrays.

INTRODUCTION

Synthetic receptors are a powerful tool for molecular recognition-based sensing. Chemosensors have a broad range of applications, such as the detection of biorelevant compounds for diagnostics, and monitoring biophysical and enzymatic processes.[1,2] An ultimate goal for synthetic sensors is to mimic the human olfactory system, containing the ability to identify many different entities from a single sensory tool.[3,4] More recently, the conceptual development of sensors has advanced towards information-rich chemical nose or cross-reactive chemosensors to achieve more prolific unique sensing profiles. This is done through either synthetic design or supramolecular assembly, combining multiple receptor and/or reporter elements into one sensing unit.[3,5] These design strategies are highlighted by examples of unimolecular probes that covalently integrate multiple complexing receptor and/or reporter components,[6,7] and biological non-covalent self-assembly-based probes that function through multi-complexing systems.[8-11]

Macrocyclic hosts are well-defined synthetic receptors for the detection of small molecules and biomacromolecules.[12-14] Host-based sensing is traditionally done using an indicator displacement assay (IDA) that operates through competitive binding of an analyte to a preformed host-indicator complex. This generally results in a fluorescence response, where sensitivity is dictated by binding affinity.[15-17] Singular host sensing systems provide limited information, typically in the form of a single output (turn-on or turn-off fluorescence) for one particular class of analyte and often fail to achieve selectivity when faced with structurally similar analytes. To attain analyte differentiation a suite of individual host-indicator sensors are often applied, where varied response patterns arise from affinity differences, producing an optical fingerprint for discrimination.[18] This strategy has been employed in macrocyclic host-based sensor arrays with some recent examples in differentiating neurotransmitters,[19] small molecule bioorganic analytes,[20] folded DNA G-quadruplexes,[21-23] insect pheromones,[24] natural amino acids,[25] and amyloid structures.[26]

The power of increasing cross-reactive self-assembly interactions is demonstrated by macrocyclic host-based chemosensors that co-assemble multiple receptor or reporter elements within the same solution. The majority of reported multi-macrocyclic host systems rely on non-specific amphiphilic aggregation to co-assemble different host classes, allowing for self-adaptable detection of larger peptide biotargets,[27] and the ability to differentiate model proteins,[28] and cells.[29] A recent report shows that macrocycles containing different integrated fluorophores have improved discrimination power when they are combined in solution, forming an adaptive network of sensors.[30] Despite these advances, further conceptual development is necessary, both through synthetic design and supramolecular assembly, in order to achieve more challenging sensing tasks.[18]

Here we present a new concept in which a mixed host chemosensor positions a single dye within a complex system, conferring the ability to generate different kinds of optical responses to hydrophobic, neutral, and cationic analytes. Supramolecular hosts tend to bind one type of guest analyte, therefore limiting the scope and applicability of any host-based sensing approach that relies on one host class.[31] In this work, we overcome this limitation by co-assembling two different classes of macrocyclic hosts, DimerDye sulfonatocalix[4]arenes and cucurbit[*n*]urils, into a single composite mixed host chemosensor (Figure 1). Key to this conceptual approach is the integration of a dye into the sulfonatocalix[4]arene scaffold, which both facilitates co-assembly and acts as a reporter for all host-host and host-analyte interactions. The equilibrium of any one pre-assembled mixed host chemosensor is poised to go in different directions depending on the nature of the analyte added, producing multi-responsive outputs, where we define multi-responsive as both "giving different photophysical responses to different analytes" and "responding to dissimilar classes of analytes" (Figure 1b). We prove the benefits of this

simple co-assembly approach in an array-based platform through the differentiation of hydrophobic, cationic, neutral and anionic drugs. We then apply these mixed host sensing systems to real-world multi-component illicit drug samples.

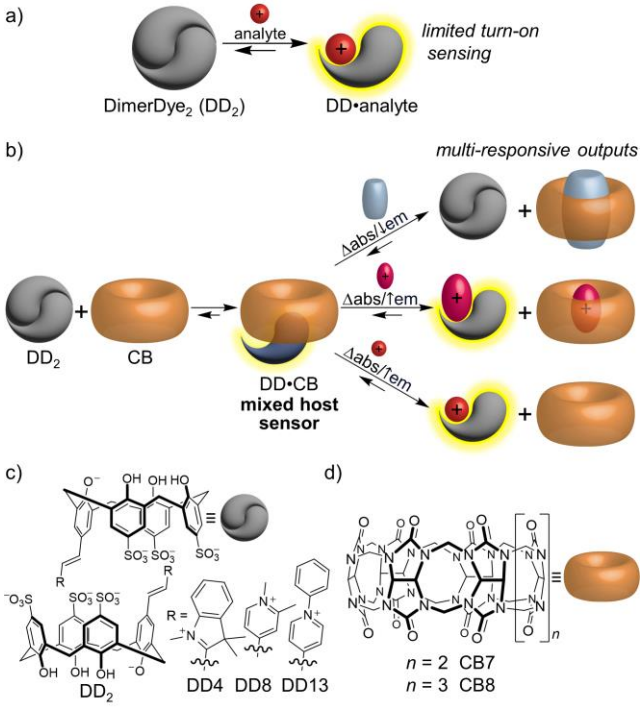

Figure 1. A mixed host chemosensor produces multi-responsive outputs, increasing the scope of analyte detection. (a) Schematic illustration of DimerDye disassembly-driven turn-on fluorescence sensing of cationic analytes. (b) This work establishes mixed host co-assembled chemosensors that produce multi-responsive outputs for a wide range of hydrophobic, neutral, and cationic analytes. DimerDye complexation with cucurbit[*n*]uril forms a mixed host chemosensor with moderate changes in absorbance/fluorescence. The subsequent addition of an analyte that favors cucurbit[*n*]uril binding produces a change in absorbance and/or turn-off fluorescence, whereas an analyte that prefers DimerDye binding results in a change in absorbance and/or increased fluorescence. The schematic shown represents the expected behaviors for CB7, while additional higher-order complexes are possible for CB8. Structures of (c) DimerDye host chemosensors DD4, DD8, and DD13, and (d) cucurbit[*n*]uril hosts CB7 and CB8 used in this work.

RESULTS AND DISCUSSION

Design of mixed host chemosensors. Two distinct host classes were selected to encourage host-host co-assembly. Previously reported DimerDye sulfonatocalix[4]arenes DD4, DD8, and DD13 (Figure 1c), [32] and cucurbit[*n*]uril hosts, CB7 and CB8 (Figure 1d) were selected to promote hetero co-assembly while contributing different analyte binding properties. Sulfonatocalix[4]arenes contain a flexible chalice-shaped cavity and negatively charged upper rim.[33] In aqueous solution the DimerDye analogs form a homodimer, stacking two fluorophores in an antiparallel quenched arrangement. Upon analyte binding, DimerDyes provide turn-on fluorescence detection through a disassembly-driven sensing mechanism (Figure 1a).[32, 34, 35] The selected DimerDyes (DD4, DD8, and DD13) cover a range of structural, absorbance, and emission properties, however, they are limited to binding cationic analytes. Conversely, cucurbit[*n*]utils have a larger range of reported analyte interactions.[36, 37] They contain a barrel-shaped rigid nonpolar cavity lined with neutral polar carbonyl portals; reporting strong binding with neutral hydrophobic guests complementary in size and shape,[38, 39] and amphiphilic cationic ammonium or diammonium guests that favor hydrophobic and ion-dipole interactions.[36] We selected CB7 and CB8 to accommodate different sized guests, where the larger CB8 cavity offers binding to bulkier hydrophobic drugs.[40, 41] We predicted the combination of these two host classes would co-assemble through hydrophobic and ion-dipole interactions from the DimerDye pendant arm binding the cucurbit[*n*]uril cavity and interacting with the polar carbonyl portals.

Mixed host co-assembly sensing mechanism. Different pairs of one DimerDye and one cucurbit[*n*]uril can co-assemble to form a mixed host chemosensor with distinct photophysical properties. Combinations of DD4•CB8, DD8•CB8, DD13•CB7, and DD13•CB8, were selected for study to understand the scope of this approach. To establish the formation of these hetero host-host complexes, changes in DimerDye absorbance and emission were monitored during titrations with increasing concentrations of cucurbit[*n*]uril. Titrations of CB8 into DD4 and CB7 into DD13 resulted in both changes in absorbance and turn-on fluorescence (Figures 2a,b and S9). These results indicate the parent DimerDye disassembles from its native homodimer state, with the turn-on fluorescence response strongly supporting the formation of a hetero-complex between the two hosts. Independently, ^{1}H NMR experiments further support the formation of hetero-complexes DD4•CB8 and DD13•CB7 by the appearance of new upfield-shifted and broadened resonances, attributed to the DimerDye pendant arm protons being in a shielded environment (Figures 2c and S10–11). The broadened CB7 peaks indicate possible aggregate formation at concentrations used in NMR, coinciding with the low solubilities of these mixed host assemblies (Figures 2c and S10–11). Upon addition of CB8, the DimerDyes DD8 and DD13, exhibited shifts in absorbance, indicating that CB8 forms a hetero-complex with DD8 and DD13 (Figure S9). However, these complexation events caused minimal changes in emission (Figure S9). In cases where both a color change and turn-on emission are observed (DD4•CB8 and DD13•CB7), we suspect the homodimer disassembly is driven by the pendant arm binding to cucurbit[*n*]uril, producing a turn-on fluorescence response. A molecular model of a possible 1:1 co-assembly of DD13 with CB7 is presented in Figure S13. In cases where only a color change is observed (DD8•CB8 and DD13•CB8) it is evident that hetero-host interactions are occurring. We suspect the non-fluorescent state is a result of assemblies where the DimerDye pendant arms are in a stacked quenched arrangement. These possible complexes include cucurbit[*n*]uril outer-surface binding interactions,[42] where multi-hetero assemblies with sulfonatocalix[4]arenes in aqueous solution have been reported,[43, 44] as well as potential ternary complexes in the larger CB8 cavity,[45-47] where two DimerDye pendant arms could potentially bind stacked inside the CB8 cavity. Irrespective of the exact complexes occurring in solution, these co-assemblies constitute different mixed host chemosensors from which distinct absorbance and fluorescence sensing outputs can arise (Figure 1b).

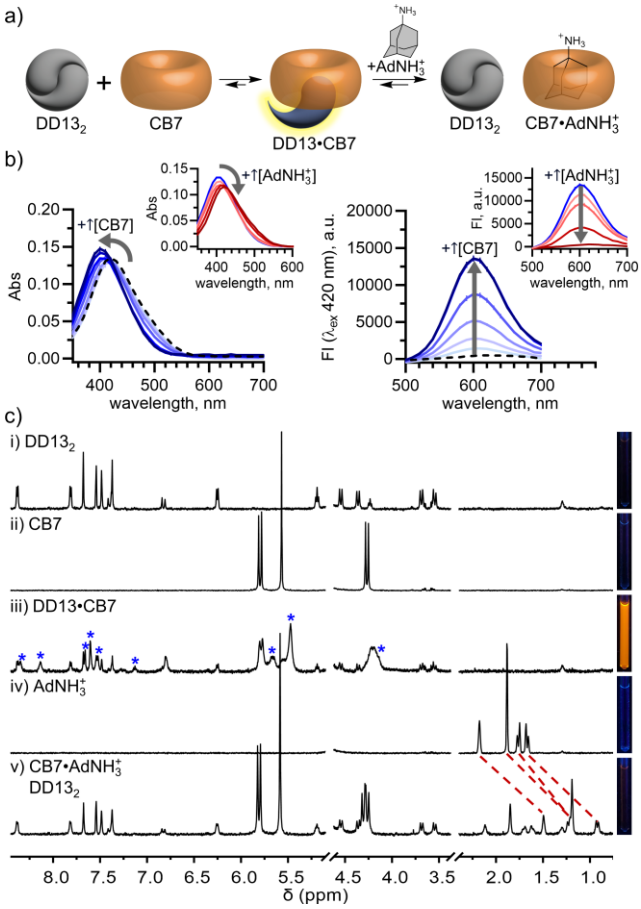

Figure 2. Mixed host DD13•CB7 co-assembly functions as a turn-off chemosensor for strong binding guests of CB7. (a) Schematic of DD13•CB7 formation and sensing mechanism of $AdNH_3^+$. (b) CB7 titration into DD13 results in a blue shift in absorbance (left) and increased fluorescence (right). Black dashed line represents DD13 (10.5 μM), light to dark blue lines represent the addition of increasing concentrations of CB7 (1.3 to 84 μM). Insets show the addition $AdNH_3^+$ to the co-assembled DD13•CB7 chemosensor induces a red shift in absorbance (left) and turn-off fluorescence (right). Blue line represents DD13 (10.5 μM) with CB7 (21 μM), light to dark red lines represent the addition of increasing concentrations of $AdNH_3^+$ (2.6 to 21 μM). All samples in NaH_2PO_4/Na_2HPO_4 (10 mM, pH 7.4) in H_2O. (c) ^{1}H NMR of iii) DD13 (100 μM) with CB7 (100 μM) shows evidence of hetero host co-assembly by the appearance of new upfield-shifted DD13 peaks and new CB7 peaks (blue stars). Disassembly of the homodimer $DD13_2$ is supported by the fluorescent appearance of the NMR tube. In v) the addition of $AdNH_3^+$ (100 μM) displaces the DD13•CB7 complex, indicated by the upfield-shifted $AdNH_3^+$ peaks (red dashed lines) and return of native homodimer $DD13_2$ peaks. The non-fluorescent appearance further supports the reformation of the homodimer $DD13_2$. All samples are in NaH_2PO_4/Na_2HPO_4 (10 mM, pD 7.4) in D_2O (500 MHz, 298 K). NMR tubes irradiated with a hand-held UV lamp (λ_{ex} 356 ± 20 nm).

Mixed host mechanistic studies with a CB-selective guest demonstrate multi-responsive emergent sensing properties that are not present in the parent chemosensor. To validate the contribution of CB's sensing responses, we selected amantadine ($AdNH_3^+$) as a high affinity guest for CB7 (K_d = 240 fM),[48] while the adamantane moiety has been shown to scarcely interact with sulfonated calixarenes.[49]

Our ^{1}H NMR experiments corroborate this, showing minimal binding of $AdNH_3^+$ to DD13 (Figure S12). In contrast, the addition of $AdNH_3^+$ to the pre-assembled moderately fluorescent co-assembled mixed host chemosensor DD13•CB7 resulted in a turn-off fluorescence response and red-shifted absorbance (Figure 2b). ^{1}H NMR studies independently confirmed the turn-off fluorescence response is due to the reformation of the quenched homodimer complex $DD13_2$ and assembly of the host-guest complex CB7•$AdNH_3^+$ (Figure 2c and S11). These results show that mixed host co-assemblies can produce photophysical responses through analyte binding to the non-fluorophore-containing host, effectively increasing the scope of analyte detection from a single sensing assembly.

Mixed host chemosensors further expand detection capabilities to new classes of analytes. On their own, DimerDyes have been reported to detect cationic illicit drugs.[32] To determine if mixed host chemosensors expand sensing abilities we selected cocaine, cannabidiol (CBD) and Vitamin C as analytes, representing cationic, neutral and anionic classes of drugs (Figure 3). As a direct comparison, we measured the fluorescence responses of the mixed host chemosensor DD13•CB7 and isolated $DD13_2$ (Figure 4). Assays with only DimerDyes provided limited information for these drugs, only producing a turn-on fluorescence response to the cationic analyte, cocaine and insignificant responses to the neutral and anionic analytes (Figure 4b). However, the mixed host chemosensor DD13•CB7 produced varied emergent responses to the different analyte classes; with increased and blue-shifted emission for cationic cocaine, decreased and blue-shifted emission for neutral CBD, and a slight, non-shifted decrease in emission to anionic Vitamin C (Figure 4a). These results highlight how the incorporation of a second host class in a self-assembled system can give varied responses to different analytes while also providing the emergent ability to detect analytes that otherwise wouldn't bind.

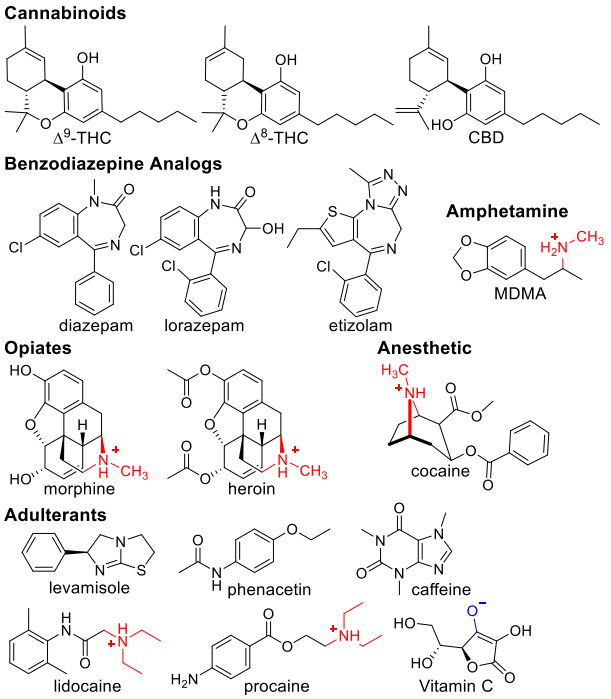

Figure 3. Chemical structures of illicit drugs and adulterants ranging in hydrophobic, neutral, cationic and anionic properties.

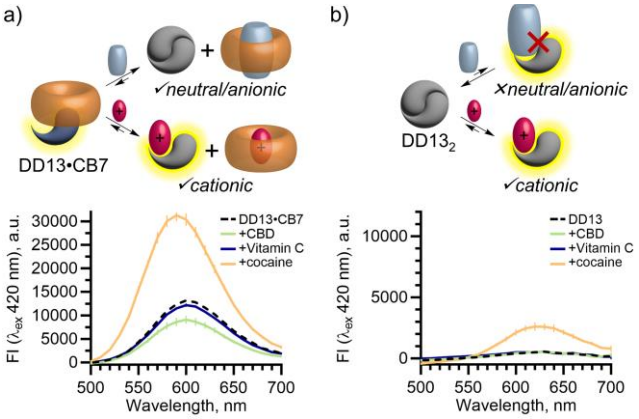

Figure 4. A mixed host chemosensor has multi-capable responses to neutral, cationic and anionic structures. (a) Fluorescence response of mixed host co-assembled chemosensor DD13•CB7 to anionic Vitamin C, neutral CBD and cationic cocaine. Samples contain [DD13] = 10.5 μM, [CB7] = 21 μM and [drug] = 105 μM. (b) Fluorescence response of isolated DD13 to anionic Vitamin C, neutral CBD and cationic cocaine. Samples contain [DD13] = 10.5 μM and [drug] = 105 μM. All samples are in NaH_2PO_4/Na_2HPO_4 (8.4 mM, pH 7.4) in H_2O with 2% MeOH.

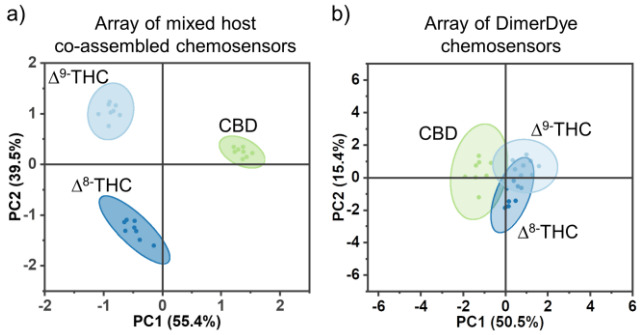

Figure 5. An array of mixed host chemosensors discriminates highly similar neutral cannabinoids. (a) PCA score plot of a mixed host co-assembled DD•CB sensor array completely discriminates CBD, Δ^8-THC and Δ^9-THC isomers. Sensor array includes absorbance and fluorescence responses of mixed host sensing pairs DD13•CB8 and DD13•CB7. Samples contain [DD] = 10.5 μM, [CB] = 21 μM and [drug] = 105 μM. (b) On their own, DimerDye chemosensors do not discriminate cannabinoids. Sensor array contains absorbance and fluorescence responses of DD4, DD8 and DD13. Samples contain [DD] = 10.5 μM and [drug] = 105 μM. PCA score plots show each sample set (n = 8) enclosed by 95% confidence ellipses. All samples are in NaH_2PO_4/Na_2HPO_4 (8.4 mM, pH 7.4) in H_2O with 2% MeOH.

Differential sensing. To further probe the power of using mixed host chemosensors, a large set of bulky, hydrophobic, cationic, neutral and anionic drugs and adulterants were selected for differentiation (Figure 3). The analytes were chosen to test the sensing range capabilities of our mixed host co-assembled chemosensors while targeting compounds commonly found in harm-reduction-based drug checking of Canadian illicit street drugs.[50] An array of mixed host chemosensors (DD4•CB8, DD8•CB8, DD13•CB8, and DD13•CB7) were screened for sensing responses, measuring select absorbance and fluorescence wavelengths (Table S1). Principal component analysis (PCA) was then used to analyze the fingerprint response patterns, aiming to discriminate samples while minimizing the number of required observations.[51]

Mixed host chemosensors can generate surprising emergent properties, including the differentiation of drugs for which neither host is considered to be a canonical binder. Cannabinoids pose a challenge for detection by supramolecular hosts as their neutral structure makes them poor guests. Hooley et. al showed that water-soluble deep cavitand sensors bind tetrahydrocannabinol (THC), and can detect and discriminate THC from its metabolites.[52] DimerDyes alone prefer cationic guests and do not give any detectable change in fluorescence response to cannabinoids (Figure 4b). Although THC has been reported not to bind CB7,[53] we found our mixed host chemosensors DD13•CB7 and DD13•CB8 each produced variable, information-rich responses. Not only was cannabinoid sensing possible from the mixed host chemosensors, but the combination of absorbance and fluorescence outputs from only two mixed host chemosensors in an array (DD13•CB7 and DD13•CB8) allowed for the complete discrimination of highly similar Δ^8- and Δ^9-THC isomers, which differ only in the position of a double bond (Figures 5a and S14). These results show that superior data-rich responses are produced from the co-assembly with cucurbit[*n*]uril hosts.

A small array of mixed host chemosensors achieves discrimination of a large set of illicit drugs and adulterants from many distinct chemical classes. We first focused on a test set containing illicit central nervous system depressants, which included both neutral benzodiazepines and cationic opiates. In this analysis, the benzodiazepines etizolam and diazepam displayed overlapping confidence ellipses while the other depressants were discriminated (Figures 5a and S16). Next, we studied a test set including cocaine and MDMA, along with a set of pharmacologically active adulterants commonly added for their synergistic effects (Figures 5b and S17).[54,55] The prescription adulterants procaine, lidocaine, levamisole, and phenacetin, were discriminated from the illicit drugs cocaine and MDMA, whereas the adulterants with fewer health repercussions, Vitamin C and caffeine, overlapped with each other. Lastly, a plot combining all tested drugs maintained similar discrimination patterns among the combined test set, with similar deficiencies in the overlap of two benzodiazepines and the adulterants Vitamin C and caffeine (Figures 5c and S18).

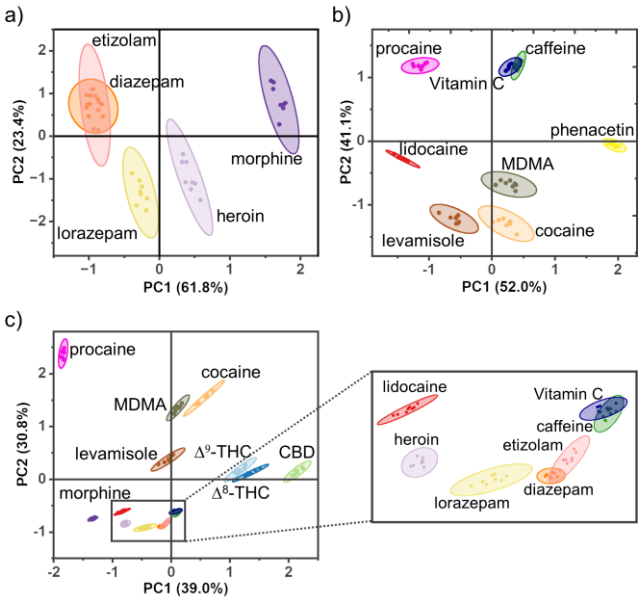

Figure 6. An array of mixed host co-assembled chemosensors distinguishes between different classes of cationic and neutral illicit drugs and adulterants. (a) PCA analysis of central nervous system depressants; neutral benzodiazepines and cationic opiates. The array of mixed host chemosensors includes absorbance and fluorescence responses from DD8•CB8, DD13•CB8 and DD13•CB7. (b) PCA plot discriminates anesthetics and amphetamine from common adulterants. The array of mixed host chemosensors includes responses from DD4•CB8, DD13•CB8, and DD13•CB7. (c) PCA analysis of all tested drugs and adulterants. The array of mixed host chemosensors includes responses from DD4•CB8, DD8•CB8, DD13•CB8 and DD13•CB7. PCA (correlation) score plot shows each sample set (n = 8) enclosed by 95% confidence ellipses. Samples contain [DD] = 10.5 μM, [CB] = 21 μM and [drug] = 105 μM. All samples are in NaH_2PO_4/Na_2HPO_4 (8.4 mM, pH 7.4) in H_2O with 2% MeOH.

Real-world illicit street drug samples represent a challenging set of multi-component targets for identification. Tests that merely reveal the presence or absence of potent substances like fentanyl are less informative tools for harm reduction in the context of the drug overdose crisis.[56] People who use drugs access drug checking services to reduce risks by obtaining an understanding of the complete composition (all active illicit drugs, adulterants, and inert compounds), with specific quantities to assess potency and dangers.[57] Currently, multiple instrument-based techniques are employed, such as combinations of immunoassay test strips, chromatography, mass spectrometry, Raman, and infrared (IR) spectroscopic methods.[58] Here we aimed to see if our mixed host chemosensors could be applied to illicit multi-component street drug samples to distinguish different composition profiles previously encountered within the drug-checking ecosystem. Street drug samples were provided by people who use drugs through Substance, the Vancouver Island Drug Checking Project,[59, 60] where drug composition and quantification were determined using Fourier transform infrared (FTIR) spectroscopy and paper spray mass spectrometry (PS-MS) (Table 1 and Figure S19). To capture the landscape of street drugs commonly in use in British Columbia, Canada, we studied representative samples from different drug classes (A-E), as well as several fentanyl-containing samples that varied slightly in composition (E-H). We also included two fentanyl samples of the same composition that arrived at the drug-checking site from two distinct users but originating from the same batch and supplier (H and I). Similar to the current protocols used for drug checking, we prepared the street drug samples for sensing experiments dissolving 1.5 mg in 1 mL methanol.[61] These stock solutions were then further diluted down to 0.03 mg/mL in all sensing experiments.

Table 1. Multi-component illicit street drug sample compositions.

Street drug sample	Composition[a]
A	Cocaine (90%), sorbitol
B	Bromazolam (>80% single component)
C	Methylenedioxymethamphetamine (MDMA, >80% single component)
D	Methylenedioxyamphetamine (MDA, 50%), dimethyl sulfone
E	Fentanyl (20%), caffeine, erythritol
F	Fentanyl (13%), fluorofentanyl (1%), caffeine
G	Fentanyl (6%), bromazolam (5%), chloroisobutyryl fentanyl (0.1%), caffeine
H*	Fentanyl (16%), fluorofentanyl (14%), 4-anilino-N-phenethyl-piperidine (ANPP, 3.7%), erythritol, caffeine
I*	Fentanyl (18%), fluorofentanyl (16%), ANPP (3.5%), erythritol, caffeine

[a]Street drug samples were acquired through Substance, the Vancouver Island Drug Checking Project, located in Victoria, Canada where sample composition was evaluated by FTIR and sample quantification was determined by PS-MS. *Samples H and I were provided by two different people who use drugs reporting the same drug from the same batch and supplier.

Mixed host chemosensors identify multi-component street drug samples where a comparable traditional sensor array cannot. Full spectral absorbance and fluorescence responses of each mixed host chemosensor (DD4•CB8, DD8•CB8, DD13•CB8 and DD13•CB7) were acquired for all multi-component street drug samples, to determine if mixed host sensing operated in more complex sample matrices (Figure S20). To provide a direct comparison to a traditional sensor array, responses of each isolated DimerDye (DD4, DD8, and DD13) were also collected (Figure S21). Mixed host chemosensors provided responses of increased emission to cationic cocaine (A), MDMA (C) and MDA (D) multi-component samples and varying decreased emission responses to neutral bromazolam (B) and various fentanyl samples (E-I) (Figure S20). In comparison, DimerDye chemosensors alone produced sensing responses smaller in amplitude, only providing increased emission responses for cationic samples A, C and D (Figure S21). Select absorbance and fluorescence wavelengths from the array of mixed host chemosensors (Table S2) were applied to PCA analysis, providing discrimination of all multi-component samples (Figure 7a and S22). The samples H and I were essentially identical by instrument-based drug checking analysis, having been reported as the same drug from the same supplier. The results of the mixed host sensor array overlap, and therefore correctly identify H and I as the same street drug sample. The same observations (Table S3) were applied to PCA analysis of the isolated DimerDye as a direct comparison of the classical single-host-class sensor array. Only discrimination of cationic samples A, C, and D were achieved, with the remaining samples (B, E-I) overlapping (Figure 7b and S23). These results show the combination of multiple host classes introduces useful variability in binding interactions. The information-rich sensing responses provide a dramatic enhancement of the overall performance.

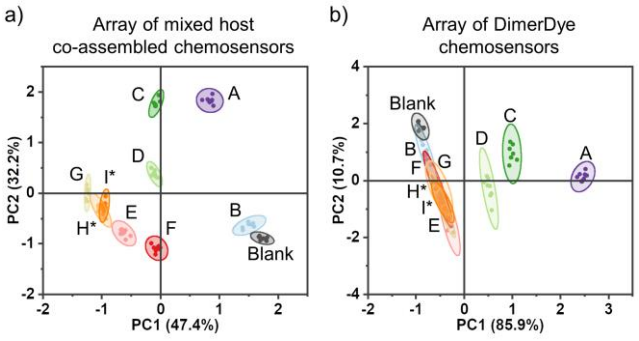

Figure 7. An array of mixed host co-assembled chemosensors discriminates multi-component street drug samples. (a) PCA analysis using absorbance and fluorescence sensor array responses from DD4•CB8, DD8•CB8, DD13•CB8, and DD13•CB7. PCA (correlation) score plot shows each samples set (n = 8) enclosed by 95% confidence ellipses. Samples contain [DD] = 10.5 μM, [CB] = 21 μM and [street drug sample] = 0.03 mg/mL. (b) DimerDye chemosensors on their own do not discriminate different multi-component street drug samples. Sensor array contains absorbance and fluorescence responses of DD4, DD8 and DD13. Samples contain [DD] = 10.5 μM and [drug] = 0.03 mg/mL. PCA score plots show each sample set (n = 8) enclosed by 95% confidence ellipses. All samples are in NaH_2PO_4/Na_2HPO_4 (8.4 mM, pH 7.4) in H_2O with 2% MeOH.

CONCLUSION

This work shows the value of increased complexity through easily co-assembled mixed host chemosensors. Interconnected equilibria are created by combining multiple binding sites of different inherent affinities within the same sensing solution. In doing so, this approach harnesses simple macrocycle combinations to generate more information-rich sensing fingerprints from a single composite sensing system. This self-assembly-based design provides a facile route to broadening the scope of analytes, where the ability to detect untargeted analytes emerges through unexpected higher-order complexation interactions. This tactic can be easily applied to a wide range of established reporter chromophores, fluorophores, and recognition binding elements, offering almost unlimited possibilities for enhancing current sensing systems. Building complexity through supramolecular assemblies can overcome some of the current limitations in host-based sensing, progressing towards challenging sensing tasks such as distinguishing complex mixture profiles, where subtle differences in multi-component mixtures are desired.

ASSOCIATED CONTENT

The Supporting Information is available free of charge at http://pubs.acs.org.

Methods and experimental procedures for absorbance and fluorescence characterization of assemblies, DFT models, ^{1}H NMR studies, absorbance and fluorescence analyte/illicit multi-component drug detection and PCA analyses (PDF)

Raw array data sets used in PCA analyses (XLSX)

AUTHOR INFORMATION

Corresponding Authors

Frank Biedermann – *Institute of Nanotechnology (INT), Karlsruhe Institute of Technology (KIT), Kaiserstraße 12, 76131 Karlsruhe, Germany*; orcid.org/0000-0002-1077-6529; Email: frank.biedermann@kit.edu

Fraser Hof – Department of Chemistry, University of Victoria, Victoria, BC V8P 5C2, Canada; Centre for Advanced Materials and Related Technology (CAMTEC), University of Victoria, Victoria, BC V8W 2Y2, Canada; orcid.org/0000-0003-4658-9132; Email: fhof@uvic.ca

Authors

Allison J. Selinger – Department of Chemistry, University of Victoria, Victoria, BC V8P 5C2, Canada; Centre for Advanced Materials and Related Technology (CAMTEC), University of Victoria, BC V8W 2Y2, Canada; orcid.org/0000-0002-7973-8686

Joana Krämer – Institute of Nanotechnology (INT), Karlsruhe Institute of Technology (KIT), Kaiserstraße 12, 76131 Karlsruhe, Germany; orcid.org/0000-0003-0498-7298

Eric Poarch – Canadian Institute for Substance Use Research, University of Victoria, Victoria, BC V8W 2Y2, Canada; orcid.org/0009-0002-7884-090X

Dennis Hore - Department of Chemistry, University of Victoria, Victoria, BC V8W 3V6, Canada; Canadian Institute for Substance Use Research, University of Victoria, Victoria, BC V8W 2Y2, Canada; Department of Computer Science, University of Victoria, Victoria, BC V8W 3P6, Canada; orcid.org/0000-0001-8969-9644

Author Contributions

‡A.J.S. and J.K. contributed equally to this work. All authors have given approval to the final version of the manuscript.

Notes

The authors declare no competing financial interest.

ACKNOWLEDGMENT

The authors thank the Natural Sciences and Engineering Research Council of Canada (NSERC, RGPIN-2019-04806) for financial support. A.J.S. thanks NSERC for the Canadian Graduate Scholarship-Doctoral (CGS-D). J.K. thanks MITACS for the Globalink Research Award. We also thank CAMTEC for the use of shared facilities and Dr. Cornelia Bohne for helpful discussion.

REFERENCES

(1) Nilam, M.; Hennig, A. Enzyme assays with supramolecular chemosensors - the label-free approach. *RSC Adv.* **2022**, *12*, 10725-10748. DOI: 10.1039/d1ra08617k.
(2) Kramer, J.; Kang, R.; Grimm, L. M.; De Cola, L.; Picchetti, P.; Biedermann, F. Molecular Probes, Chemosensors, and Nanosensors for Optical Detection of Biorelevant Molecules and Ions in Aqueous Media and Biofluids. *Chem. Rev.* **2022**, *122*, 3459-3636. DOI: 10.1021/acs.chemrev.1c00746.
(3) Geng, Y.; Peveler, W. J.; Rotello, V. M. Array-based "Chemical Nose" Sensing in Diagnostics and Drug Discovery. *Angew. Chem. Int. Ed.* **2019**, *58*, 5190-5200. DOI: 10.1002/anie.201809607.
(4) Guerrini, L.; Garcia-Rico, E.; Pazos-Perez, N.; Alvarez-Puebla, R. A. Smelling, Seeing, Tasting—Old Senses for New Sensing. *ACS Nano* **2017**, *11*, 5217-5222. DOI: 10.1021/acsnano.7b03176.
(5) Motiei, L.; Margulies, D. Molecules That Generate Fingerprints: A New Class of Fluorescent Sensors for Chemical Biology, Medical Diagnosis, and Cryptography. *Acc. Chem. Res.* **2023**, *56*, 1803-1814. DOI: 10.1021/acs.accounts.3c00162.
(6) Rout, B.; Unger, L.; Armony, G.; Iron, M. A.; Margulies, D. Medication Detection by a Combinatorial Fluorescent Molecular Sensor. *Angew. Chem. Int. Ed.* **2012**, *51*, 12477-12481. DOI: 10.1002/anie.201206374.
(7) Pode, Z.; Peri-Naor, R.; Georgeson, J. M.; Ilani, T.; Kiss, V.; Unger, T.; Markus, B.; Barr, H. M.; Motiei, L.; Margulies, D. Protein Recognition by a Pattern-Generating Fluorescent Molecular Probe. *Nat. Nanotechnol.* **2017**, *12*, 1161-1168. DOI: 10.1038/nnano.2017.175.
(8) De, M.; Rana, S.; Akpinar, H.; Miranda, O. R.; Arvizo, R. R.; Bunz, U. H. F.; Rotello, V. M. Sensing of Proteins in Human Serum Using Conjugates of Nanoparticles and Green Fluorescent Protein. *Nat. Chem.* **2009**, *1*, 461-465. DOI: 10.1038/nchem.334.
(9) Rana, S.; Le, N. D. B.; Mout, R.; Saha, K.; Tonga, G. Y.; Bain, R. E. S.; Miranda, O. R.; Rotello, C. M.; Rotello, V. M. A Multichannel Nanosensor for Instantaneous Readout of Cancer Drug Mechanisms. *Nat. Nanotechnol.* **2015**, *10*, 65-69. DOI: 10.1038/nnano.2014.285.
(10) Geng, Y.; Amante, J. J.; Goel, H. L.; Zhang, X.; Walker, M. R.; Luther, D. C.; Mercurio, A. M.; Rotello, V. M. Differentiation of Cancer Stem Cells Through Nanoparticle Surface Engineering. *ACS Nano* **2020**, *14*, 15276-15285. DOI: 10.1021/acsnano.0c05589.
(11) Peri-Naor, R.; Pode, Z.; Lahav-Mankovski, N.; Rabinkov, A.; Motiei, L.; Margulies, D. Glycoform Differentiation by a Targeted, Self-Assembled, Pattern-Generating Protein Surface Sensor. *J. Am. Chem. Soc.* **2020**, *142*, 15790-15798. DOI: 10.1021/jacs.0c05644.
(12) Pan, Y. C.; Tian, J. H.; Guo, D. S. Molecular Recognition with Macrocyclic Receptors for Application in Precision Medicine. *Acc. Chem. Res.* **2023**, *56*, 3626-3639. DOI: 10.1021/acs.accounts.3c00585.
(13) Chen, J.; Hooley, R. J.; Zhong, W. Applications of Synthetic Receptors in Bioanalysis and Drug Transport. *Bioconjug. Chem.* **2022**, *33*, 2245-2253. DOI: 10.1021/acs.bioconjchem.2c00096.
(14) Pinalli, R.; Pedrini, A.; Dalcanale, E. Biochemical sensing with macrocyclic receptors. *Chem. Soc. Rev.* **2018**, *47*, 7006-7026. DOI: 10.1039/c8cs00271a.
(15) Nguyen, B. T.; Anslyn, E. V. Indicator–Displacement Assays. *Coord. Chem. Rev.* **2006**, *250*, 3118-3127. DOI: 10.1016/j.ccr.2006.04.009.
(16) Sedgwick, A. C.; Brewster, J. T.; Wu, T.; Feng, X.; Bull, S. D.; Qian, X.; Sessler, J. L.; James, T. D.; Anslyn, E. V.; Sun, X. Indicator displacement assays (IDAs): the past, present and future. *Chem. Soc. Rev.* **2021**, *50*, 9-38. DOI: 10.1039/c9cs00538b.
(17) Dsouza, R. N.; Pischel, U.; Nau, W. M. Fluorescent dyes and their supramolecular host/guest complexes with macrocycles in aqueous solution. *Chem. Rev.* **2011**, *111*, 7941-7980. DOI: 10.1021/cr200213s.
(18) Fargher, H. A.; D'Oelsnitz, S.; Diaz, D. J.; Anslyn, E. V. Pushing Differential Sensing Further: The Next Steps in Design and Analysis of Bio-Inspired Cross-Reactive Arrays. *Anal. Sens.* **2023**, *3*, e202200095. DOI: 10.1002/anse.202200095.
(19) Mei, Y.; Zhang, Q. W.; Gu, Q.; Liu, Z.; He, X.; Tian, Y. Pillar[5]arene-Based Fluorescent Sensor Array for Biosensing of Intracellular Multi-neurotransmitters through Host-Guest Recognitions. *J. Am. Chem. Soc.* **2022**, *144*, 2351-2359. DOI: 10.1021/jacs.1c12959.
(20) Hu, C.; Jochmann, T.; Chakraborty, P.; Neumaier, M.; Levkin, P. A.; Kappes, M. M.; Biedermann, F. Further Dimensions for Sensing in Biofluids: Distinguishing Bioorganic Analytes by the Salt-Induced Adaptation of a Cucurbit[7]uril-Based Chemosensor. *J. Am.Chem. Soc.* **2022**, *144*, 13084-13095. DOI: 10.1021/jacs.2c01520.
(21) Chen, J.; Hickey, B. L.; Gao, Z.; Raz, A. A. P.; Hooley, R. J.; Zhong, W. Sensing Base Modifications in Non-Canonically Folded DNA with an Optimized Host:Guest Sensing Array. *ACS Sensors* **2022**, *7*, 2164-2169. DOI: 10.1021/acssensors.2c00839.
(22) Chen, J.; Gill, A. D.; Hickey, B. L.; Gao, Z.; Cui, X.; Hooley, R. J.; Zhong, W. Machine learning aids classification and discrimination of noncanonical DNA folding motifs by an arrayed host:guest sensing system. *J. Am. Chem. Soc.* **2021**, *143*, 12791-12799. DOI: 10.1021/jacs.1c06031.
(23) Chen, J.; Hickey, B. L.; Wang, L.; Lee, J.; Gill, A. D.; Favero, A.; Pinalli, R.; Dalcanale, E.; Hooley, R. J.; Zhong, W. Selective discrimination and classification of G-quadruplex structures with a host–guest sensing array. *Nat. Chem.* **2021**, *13*, 488-495. DOI: 10.1038/s41557-021-00647-9.
(24) Hickey, B. L.; Chen, J.; Zou, Y.; Gill, A. D.; Zhong, W.; Millar, J. G.; Hooley, R. J. Enantioselective Sensing of Insect Pheromones in Water. *Chem. Comm.* **2021**, *57*, 13341-13344. DOI: 10.1039/d1cc05540b.
(25) Wang, B.; Han, J.; Bojanowski, N. M.; Bender, M.; Ma, C.; Seehafer, K.; Herrmann, A.; Bunz, U. H. F. An Optimized Sensor Array Identifies All Natural Amino Acids. *ACS Sens.* **2018**, *3*, 1562-1568. DOI: 10.1021/acssensors.8b00371.
(26) Das Saha, N.; Pradhan, S.; Sasmal, R.; Sarkar, A.; Berač, C. M.; Kölsch, J. C.; Pahwa, M.; Show, S.; Rozenholc, Y.; Topçu, Z.; et al.

Cucurbit[7]uril Macrocyclic Sensors for Optical Fingerprinting: Predicting Protein Structural Changes to Identifying Disease-Specific Amyloid Assemblies. *J. Am. Chem. Soc.* **2022**, *144*, 14363-14379. DOI: 10.1021/jacs.2c05969.
(27) Xu, Z.; Jia, S.; Wang, W.; Yuan, Z.; Jan Ravoo, B.; Guo, D.-S. Heteromultivalent Peptide Recognition by Co-assembly of Cyclodextrin and Calixarene Amphiphiles Enables Inhibition of Amyloid Fibrillation. *Nat. Chem.* **2019**, *11*, 86-93. DOI: 10.1038/s41557-018-0164-y.
(28) Tian, J. H.; Hu, X. Y.; Hu, Z. Y.; Tian, H. W.; Li, J. J.; Pan, Y. C.; Li, H. B.; Guo, D. S. A Facile Way to Construct Sensor Array Library via Supramolecular Chemistry for Discriminating Complex Systems. *Nat. Commun.* **2022**, *13*, 4293. DOI: 10.1038/s41467-022-31986-x.
(29) Hu, X. Y.; Hu, Z. Y.; Tian, J. H.; Shi, L.; Ding, F.; Li, H. B.; Guo, D. S. A Heteromultivalent Host-Guest Sensor Array for Cell Recognition and Discrimination. *Chem. Commun.* **2022**, *58*, 13198-13201. DOI: 10.1039/d2cc04963e.
(30) Selinger, A. J.; Hof, F. Adaptive Supramolecular Networks: Emergent Sensing from Complex Systems. *Angew. Chem. Int. Ed.* **2023**, *62*, e202312407. DOI: 10.1002/anie.202312407.
(31) Zhong, W.; Hooley, R. J. Combining Excellent Selectivity with Broad Target Scope: Biosensing with Arrayed Deep Cavitand Hosts. *Acc. Chem. Res.* **2022**, *55*, 1035-1046. DOI: 10.1021/acs.accounts.2c00026.
(32) Beatty, M. A.; Selinger, A. J.; Li, Y.; Hof, F. Parallel Synthesis and Screening of Supramolecular Chemosensors that Achieve Fluorescent Turn-on Detection of Drugs in Saliva. *J. Am. Chem. Soc.* **2019**, *141*, 16763-16771. DOI: 10.1021/jacs.9b07073.
(33) Guo, D.-S.; Wang, K.; Liu, Y. Selective Binding Behaviors of *p*-Sulfonatocalixarenes in Aqueous Solution. *J. Incl. Phenom. Macrocycl. Chem.* **2008**, *62*, 1-21. DOI: 10.1007/s10847-008-9452-2.
(34) Beatty, M. A.; Borges-González, J.; Sinclair, N. J.; Pye, A. T.; Hof, F. Analyte-Driven Disassembly and Turn-On Fluorescent Sensing in Competitive Biological Media. *J. Am. Chem. Soc.* **2018**, *140*, 3500-3504. DOI: 10.1021/jacs.7b13298.
(35) Gallo, C.; Thomas, S. S.; Selinger, A. J.; Hof, F.; Bohne, C. Mechanism of a Disassembly-Driven Sensing System Studied by Stopped-Flow Kinetics. *J. Org. Chem.* **2021**, *86*, 10782-10787. DOI: 10.1021/acs.joc.1c00959.
(36) Barrow, S. J.; Kasera, S.; Rowland, M. J.; Del Barrio, J.; Scherman, O. A. Cucurbituril-Based Molecular Recognition. *Chem. Rev.* **2015**, *115*, 12320-12406. DOI: 10.1021/acs.chemrev.5b00341.
(37) Sinn, S.; Biedermann, F. Chemical Sensors Based on Cucurbit[n]uril Macrocycles. *Isr. J. Chem.* **2018**, *58*, 357-412. DOI: 10.1002/ijch.201700118.
(38) Assaf, K. I.; Nau, W. M. Cucurbiturils: from Synthesis to High-affinity Binding and Catalysis. *Chem. Soc. Rev.* **2015**, *44*, 394-418. DOI: 10.1039/c4cs00273c.
(39) Lazar, A. I.; Biedermann, F.; Mustafina, K. R.; Assaf, K. I.; Hennig, A.; Nau, W. M. Nanomolar Binding of Steroids to Cucurbit[*n*]urils: Selectivity and Applications. *J. Am. Chem. Soc.* **2016**, *138*, 13022-13029. DOI: 10.1021/jacs.6b07655.
(40) Murkli, S.; Klemm, J.; Brockett, A. T.; Shuster, M.; Briken, V.; Roesch, M. R.; Isaacs, L. In Vitro and In Vivo Sequestration of Phencyclidine by Me_4Cucurbit[8]uril. *Chem. Eur. J.* **2021**, *27*, 3098-3105. DOI: 10.1002/chem.202004380.
(41) Das, D.; Assaf, K. I.; Nau, W. M. Applications of Cucurbiturils in Medicinal Chemistry and Chemical Biology. *Front. Chem.* **2019**, *7*, 619. DOI: 10.3389/fchem.2019.00619.
(42) Huang, Y.; Gao, R. H.; Liu, M.; Chen, L. X.; Ni, X. L.; Xiao, X.; Cong, H.; Zhu, Q. J.; Chen, K.; Tao, Z. Cucurbit[*n*]uril-Based Supramolecular Frameworks Assembled Through Outer-Surface Interactions. *Angew. Chem. Int. Ed.* **2021**, *60*, 15166-15191. DOI: 10.1002/anie.202002666.
(43) Tian, X.; Chen, L. X.; Yao, Y. Q.; Chen, K.; Chen, M.-D.; Zeng, X.; Tao, Z. 4-Sulfocalix[4]arene/Cucurbit[7]uril-Based Supramolecular Assemblies Through the Outer Surface Interactions of Cucurbit[*n*]uril. *ACS Omega* **2018**, *3*, 6665-6672. DOI: 10.1021/acsomega.8b00829.
(44) Lin, R.-G.; Long, L.-S.; Huang, R.-B.; Zheng, L.-S. Directing Role of Hydrophobic–Hydrophobic and Hydrophilic–Hydrophilic Interactions in the Self-Assembly of Calixarenes/Cucurbiturils-Based Architectures. *Cryst. Growth Des.* **2008**, *8*, 791-794. DOI: 10.1021/cg701084x.
(45) Liu, J.; Lambert, H.; Zhang, Y.-W.; Lee, T.-C. Rapid Estimation of Binding Constants for Cucurbit[8]uril Ternary Complexes Using Electrochemistry. *Anal. Chem.* **2021**, *93*, 4223-4230. DOI: 10.1021/acs.analchem.0c04887.
(46) Biedermann, F.; Ross, I.; Scherman, O. A. Host–guest accelerated photodimerisation of anthracene-labeled macromolecules in water. *Polym. Chem.* **2014**, *5*. DOI: 10.1039/c4py00627e.
(47) Sayed, M.; Biedermann, F.; Uzunova, V. D.; Assaf, K. I.; Bhasikuttan, A. C.; Pal, H.; Nau, W. M.; Mohanty, J. Triple emission from p-dimethylaminobenzonitrile-cucurbit[8]uril triggers the elusive excimer emission. *Chem. Eur. J.* **2015**, *21*, 691-696. DOI: 10.1002/chem.201404902.
(48) Liu, S.; Ruspic, C.; Mukhopadhyay, P.; Chakrabarti, S.; Zavalij, P. Y.; Isaacs, L. The Cucurbit[n]uril Family: Prime Components for Self-Sorting Systems. *J. Am. Chem. Soc.* **2005**, *127*, 15959-15967. DOI: 10.1021/ja055013x.
(49) Zhao, H.-X.; Guo, D.-S.; Wang, L.-H.; Qian, H.; Liu, Y. A Novel Supramolecular Ternary Polymer with Two Orthogonal Host–guest Interactions. *Chem. Commun.* **2012**, *48*, 11319. DOI: 10.1039/c2cc34834a.
(50) Belzak, L.; Halverson, J. Evidence synthesis - The opioid crisis in Canada: a national perspective. *Health Promot. Chronic Dis. Prev. Can.* **2018**, *38*, 224-233. DOI: 10.24095/hpcdp.38.6.02.
(51) Stewart, S.; Ivy, M. A.; Anslyn, E. V. The use of principal component analysis and discriminant analysis in differential sensing routines. *Chem. Soc. Rev.* **2014**, *43*, 70-84. DOI: 10.1039/c3cs60183h.
(52) Gill, A. D.; Hickey, B. L.; Zhong, W.; Hooley, R. J. Selective Sensing of THC and Related Metabolites in Biofluids by Host:Guest Arrays. *Chem. Comm.* **2020**, *56*, 4352-4355. DOI: 10.1039/d0cc01489c.
(53) Du, X.; Hao, H.; Qin, A.; Tang, B. Z. Highly Sensitive Chemosensor for Detection of Methamphetamine by the Combination of AIE Luminogen and Cucurbit[7]uril. *Dyes Pigm.* **2020**, *180*. DOI: 10.1016/j.dyepig.2020.108413.
(54) Cole, C.; Jones, L.; McVeigh, J.; Kicman, A.; Syed, Q.; Bellis, M. Adulterants in illicit drugs: a review of empirical evidence. *Drug Test Anal.* **2011**, *3*, 89-96. DOI: 10.1002/dta.220.
(55) C. Cole, L. J., J. McVeigh, A. Kicman, Q. Syed, M.A. Bellis. *Cut: a guide to adulterants, bulking agents and other contaminants found in illicit drugs.*; Liverpool John Moores University, Liverpool, 2010.
(56) Halifax, J. C.; Lim, L.; Ciccarone, D.; Lynch, K. L. Testing the test strips: laboratory performance of fentanyl test strips. *Harm Reduct. J.* **2024**, *21*. DOI: 10.1186/s12954-023-00921-8.

(57) Ivsins, A.; Boyd, J.; Beletsky, L.; McNeil, R. Tackling the Overdose Crisis: The Role of Safe Supply. *Int. J. Drug Policy* **2020**, *80*, 102769. DOI: 10.1016/j.drugpo.2020.102769.
(58) Gozdzialski, L.; Wallace, B.; Hore, D. Point-of-care Community Drug Checking Technologies: an Insider Look at the Scientific Principles and Practical Considerations. *Harm Reduct. J.* **2023**, *20*. DOI: 10.1186/s12954-023-00764-3.
(59) Wallace, B.; Hills, R.; Rothwell, J.; Kumar, D.; Garber, I.; Van Roode, T.; Larnder, A.; Pagan, F.; Aasen, J.; Weatherston, J.; et al. Implementing an integrated multi-technology platform for drug checking: Social, scientific, and technological considerations. *Drug Test Anal.* **2021**, *13*, 734-746. DOI: 10.1002/dta.3022.
(60) Wallace, B.; Gozdzialski, L.; Qbaich, A.; Shafiul, A.; Burek, P.; Hutchison, A.; Teal, T.; Louw, R.; Kielty, C.; Robinson, D.; et al. A distributed model to expand the reach of drug checking. *Drugs Habits Soc. Pol.* **2022**, *23*, 220-231. DOI: 10.1108/dhs-01-2022-0005.
(61) Borden, S. A.; Saatchi, A.; Vandergrift, G. W.; Palaty, J.; Lysyshyn, M.; Gill, C. G. A New Quantitative Drug Checking Technology for Harm Reduction: Pilot Study in Vancouver, Canada Using Paper Spray Mass Spectrometry. *Drug Alcohol Rev.* **2022**, *41*, 410-418. DOI: 10.1111/dar.13370.

Supporting Information

Table of Contents:

1. General methods and materials

1.1 Materials

The following chemicals were used as received without further purification. Cucurbit[7]uril hydrate (CB7), berberine chloride (BC), phenacetin (≥98.0%), procaine hydrochloride (≥97%), lidocaine hydrochloride monohydrate and levamisole hydrochloride were purchased from Sigma Aldrich. L-ascorbic acid (≥99.0%) was purchased from Fisher Scientific. 1-Adamantanamine ($AdNH_3^+$) hydrochloride (≥99.0%) was purchased from TCI. Analytical drug samples from Cerilliant® were purchased through Sigma Aldrich as 1 mg/mL ampules in methanol or acetonitrile: morphine solution, diazepam solution, etizolam solution, cannabidiol (CBD) solution, Δ^9-tetrahydrocannabinol (Δ^9-THC) solution, (−)-Δ^8- tetrahydrocannabinol (Δ^8-THC) solution, (±)-3,4-methylenedioxymethamphetamine (MDMA) solution, cocaine hydrochloride solution, heroin solution and lorazepam solution.

The DimerDyes DD4, DD8, and DD13 were synthesized and purified following reported protocols.[1] Cucurbit[8]uril (CB8) was synthesized and purified following literature procedures.[2, 3] *N,N'*-dimethyl-2,7-diazapyrenium diiodide (MDAP) was synthesized and purified following the reported protocol.[4]

Street drug samples were collected from Substance, the Vancouver Island Drug Checking Project, located in Victoria, BC, Canada.[5, 6] Solid samples (<10 mg) were submitted by people who use drugs as part of the drug checking service and were analyzed at Substance using established protocols. Fourier transform infrared (FTIR) spectra were collected using a 45° single-bounce attenuated total reflection (ATR) element. The resulting IR spectra were analyzed using classification models for the presence or absence of trace actives.[7] Paper spray-mass spectrometry (PS-MS) analysis was performed to confirm the presence of select target compounds and to provide quantitative concentration information.[8-11] Cases where measurements were above the limit of quantification are reported as >80%, where the lower limit of quantification is approximately 0.1% (weight/weight).[5]

1.2 General UPLC-MS and NMR spectroscopy methods

DimerDye purity was verified using a Waters UPLC-MS equipped with an Acquity UPLC BEH C18 1.7 µm (21 x 50 mm) column, UV/Vis and QDa detector. A gradient of 90% H_2O (0.4% CH_2O_2)/10% CH_3CN (0.4% CH_2O_2) to 30% H_2O (0.4% CH_2O_2)/70% CH_3CN (0.4% CH_2O_2) over 5 minutes at 0.5 mL/min flow was used for all purity traces. All NMR spectra were recorded on a Bruker Avance Neo 500 at 298 K (^{1}H: 500 MHz). ^{1}H NMR performed in phosphate buffer (50 mM, pD 7.4) was prepared using sodium phosphate monobasic and sodium phosphate dibasic in D_2O. The pD was adjusted with 1 M NaOD/DCl and determined using a pH meter.[12]

1.3 General sample preparation for absorbance and fluorescence

Stock solutions of cucurbit[*n*]uril hosts CB7 and CB8 and dyes MDAP and BC were prepared in Milli-Q™ ultrapure water. The concentrations of stock dye solutions MDAP and BC were determined by UV-Vis titration measurements using the reported extinction coefficients (BC, $\varepsilon_{344\ nm} = 22300\ M^{-1}cm^{-1}$ and MDAP, $\varepsilon_{393\ nm} = 7800\ M^{-1}cm^{-1}$) and Beer-Lambert Law.[13-15] The concentration of cucurbit[*n*]uril stock solutions (CB7 and CB8) was determined in H_2O following reported titration protocols with known strong binding dyes (MDAP and BC, respectively).[13, 14] CB7 was titrated into MDAP, recording the emission at $\lambda_{em} = 454$ nm ($\lambda_{ex} = 393$ nm). CB8 was titrated into BC, recording the emission at $\lambda_{em} = 542$ nm ($\lambda_{ex} = 421$ nm). Stock solutions of DimerDyes (1 mM) were prepared by mass in NaH_2PO_4/Na_2HPO_4 (10 mM, pH 7.4) in H_2O. Analytical drug ampules were evaporated overnight under a gentle air stream and redissolved in methanol to form 5.2 mM stock solutions. Solid street drug samples were dissolved in analytical-grade methanol to form 1.5 mg/mL stock solutions.

2. Macrocyclic host synthesis and purity – ^{1}H NMR and UPLC-MS

The calixarene intermediate sCx4-CHO was synthesized following reported protocols.[16] DimerDyes DD4, DD8 and DD13 were synthesized and purified following reported protocols.[1]

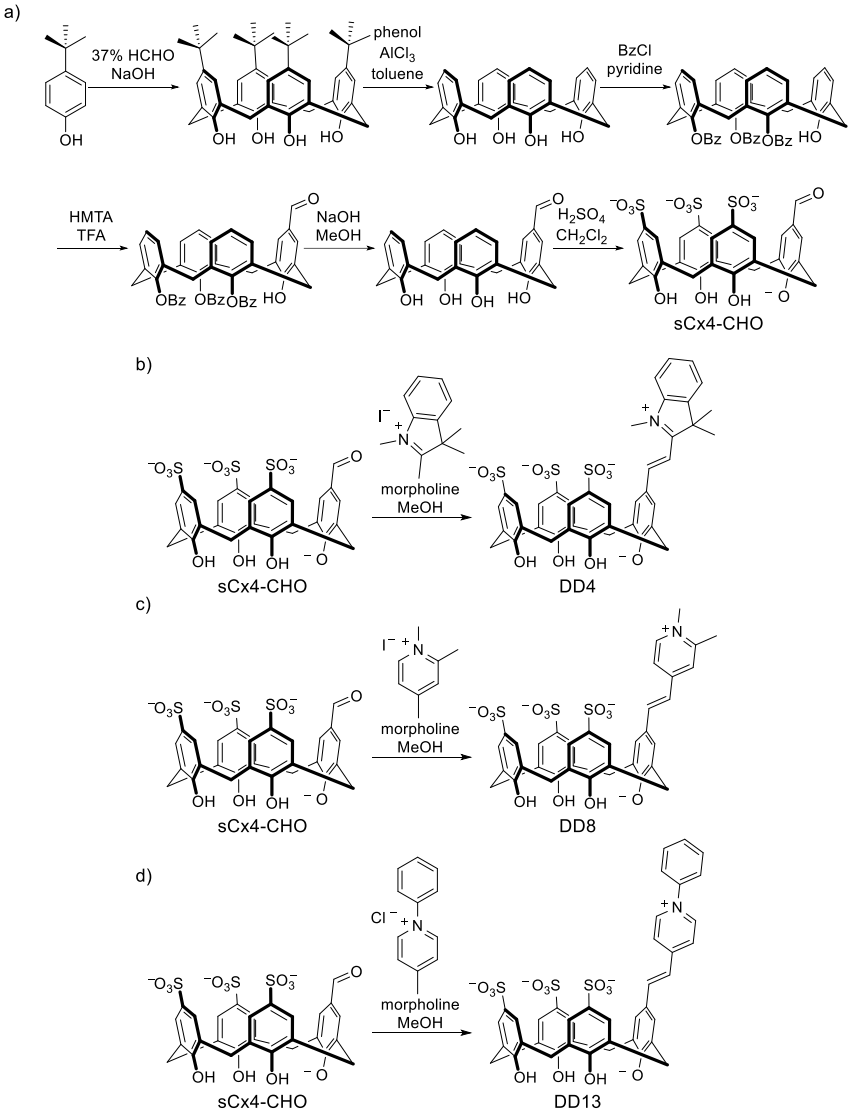

Scheme S1. Synthetic route of (a) intermediate sCx4-CHO and synthesis of (b) DD4 (c) DD8 and (d) DD13.[1, 16]

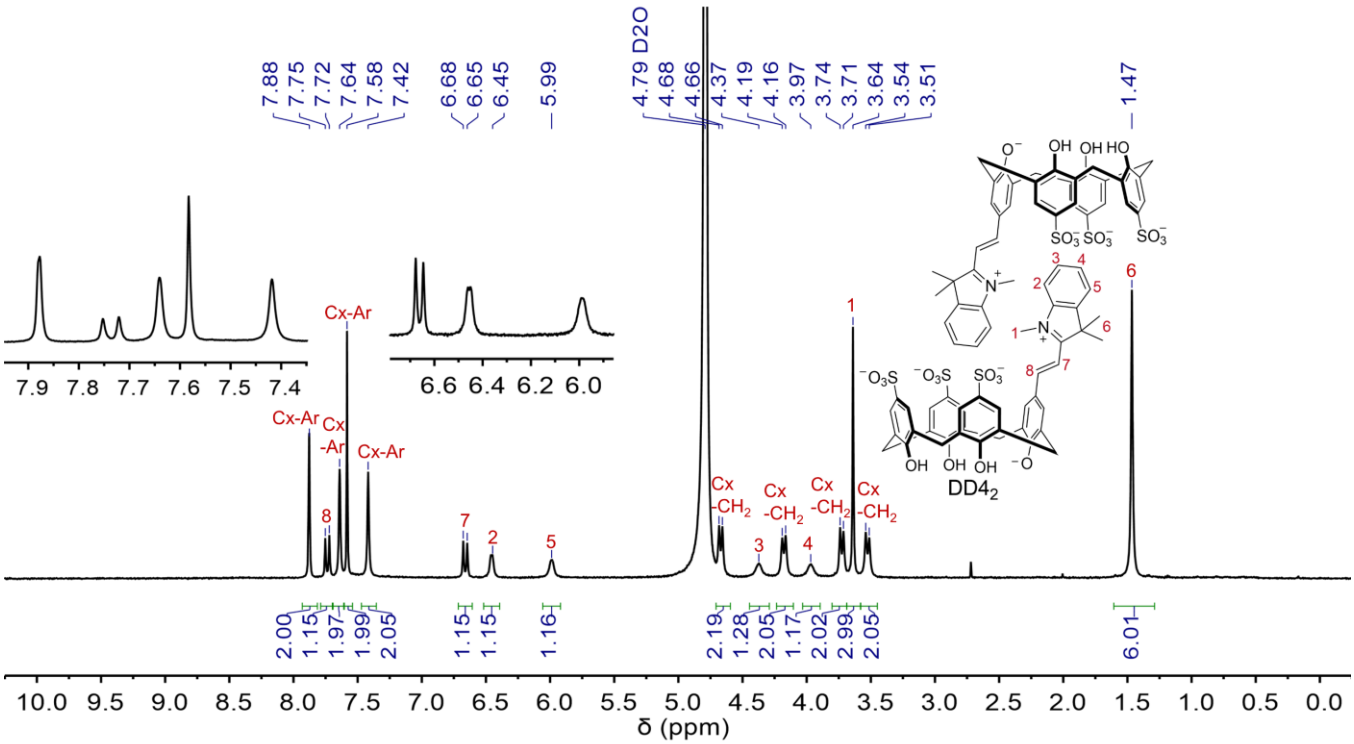

Figure S1. ^{1}H NMR spectrum of $DD4_2$ in NaH_2PO_4/Na_2HPO_4 (50 mM, pD 7.4) in D_2O (500 MHz, 298 K) shows upfield shifted pendant arm methyl and aromatic protons, supporting the existence of the molecule as a homodimer in aqueous solution.

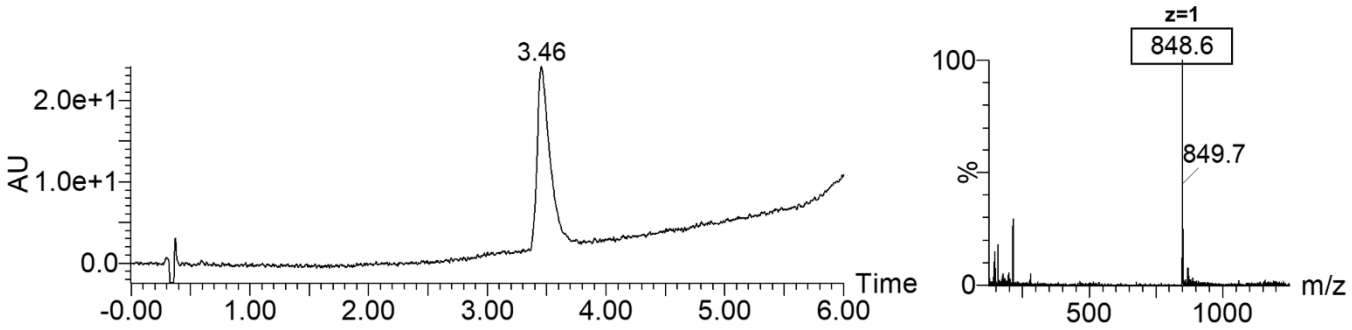

Figure S2. UPLC-MS (ES+) of DD4. Left = UV diode array detected chromatogram (190:400 nm). Right = positive ion mode ESI mass spectrum of the eluted peak.

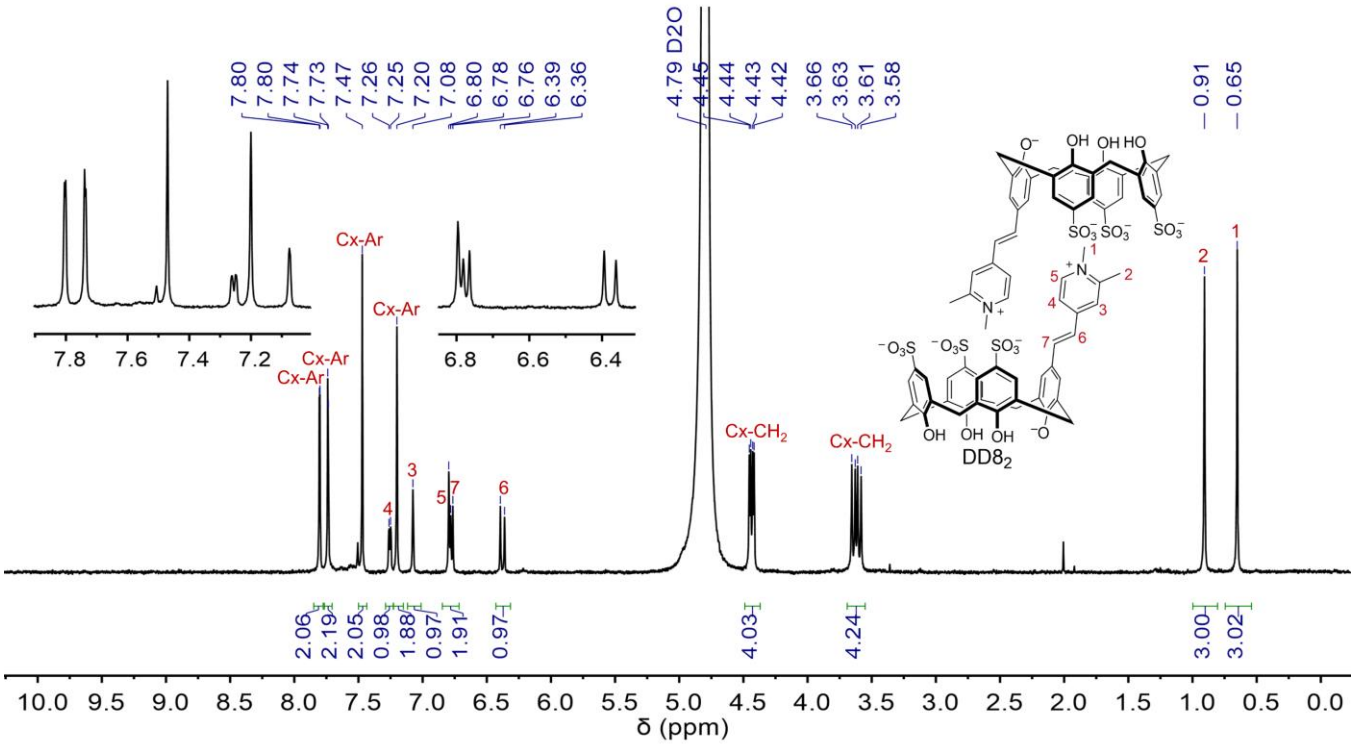

Figure S3. ^{1}H NMR spectrum of $DD8_2$ in NaH_2PO_4/Na_2HPO_4 (50 mM, pD 7.4) in D_2O (500 MHz, 298 K) shows upfield shifted pendant arm methyl and aromatic protons, supporting the existence of the molecule as a homodimer in aqueous solution.

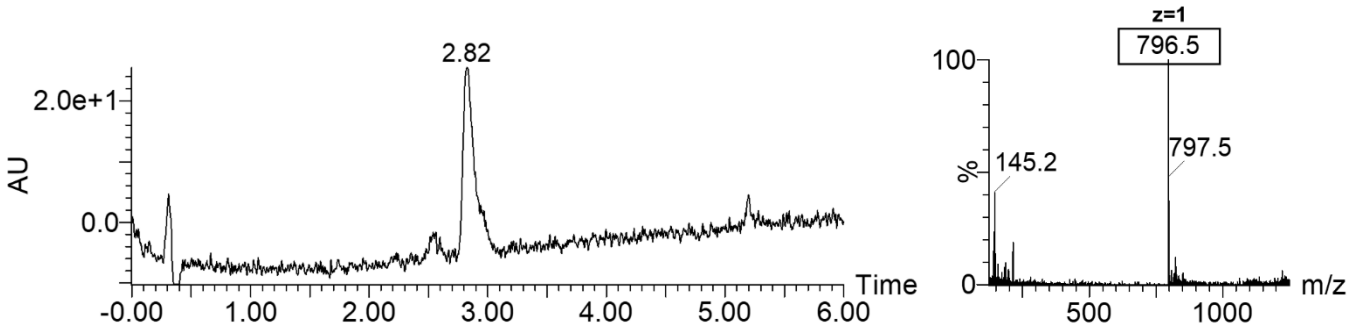

Figure S4. UPLC-MS (ES+) of DD8. Left = UV diode array detected chromatogram (190:800 nm). Right = positive ion mode ESI mass spectrum of the eluted peak.

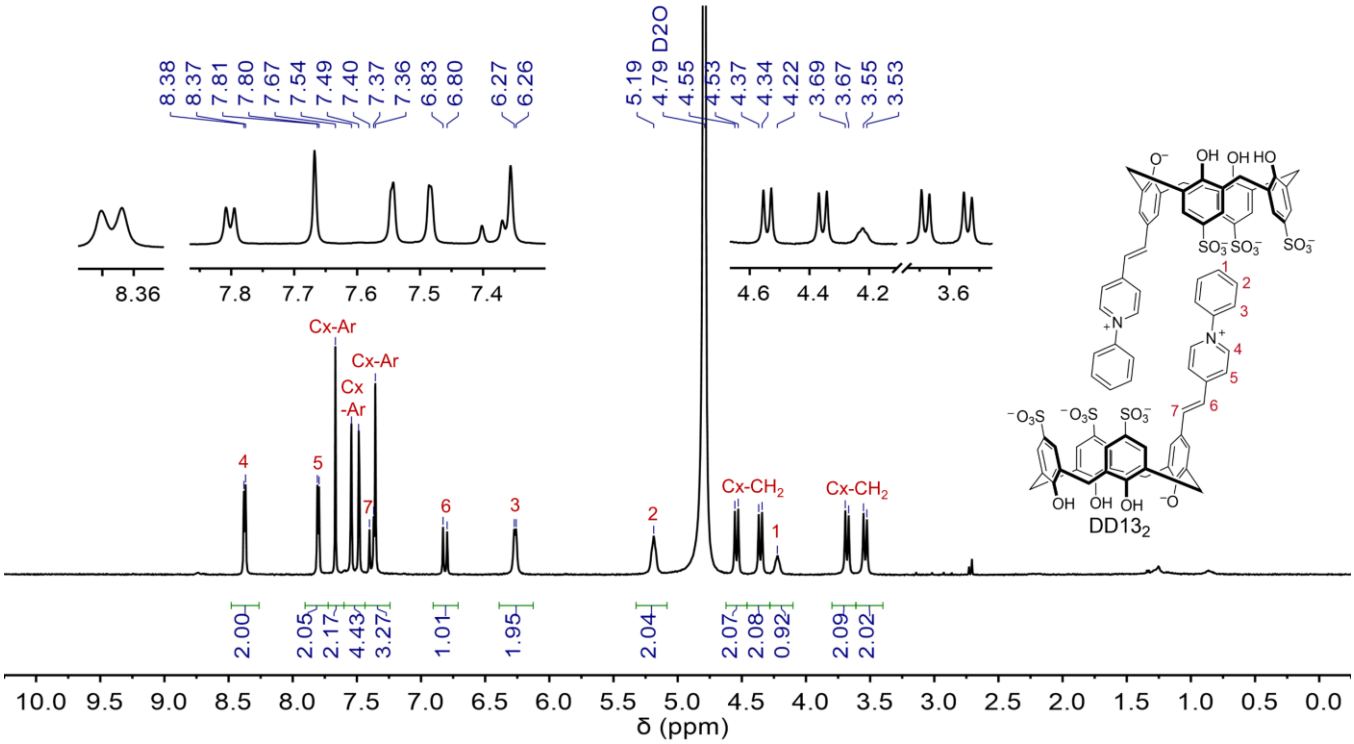

Figure S5. ^{1}H NMR spectrum of $DD13_2$ in NaH_2PO_4/Na_2HPO_4 (50 mM, pD 7.4) in D_2O (500 MHz, 298 K) shows upfield shifted pendant arm aromatic protons, supporting the existence of the molecule as a homodimer in aqueous solution.

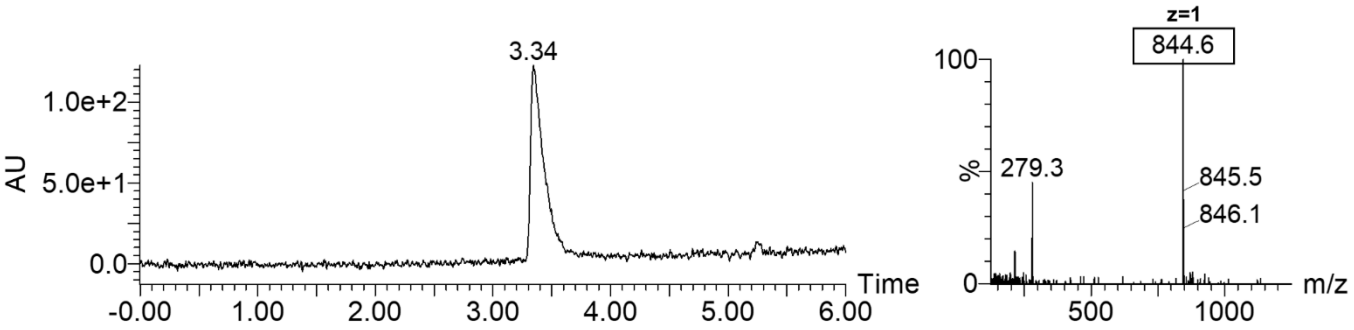

Figure S6. UPLC-MS (ES+) of DD13. Left = UV diode array detected chromatogram (190:800 nm). Right = positive ion mode ESI mass spectrum of the eluted peak.

Cucurbit[8]uril (CB8) was synthesized using literature methods.[2]

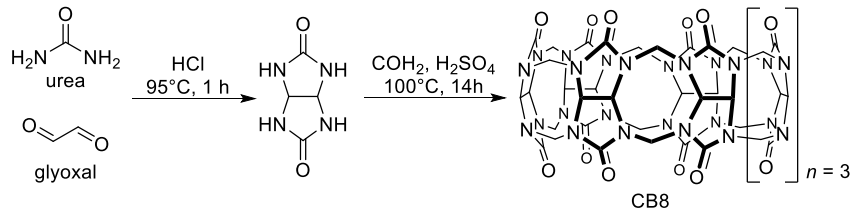

Scheme S2. Synthetic route of CB8.[2]

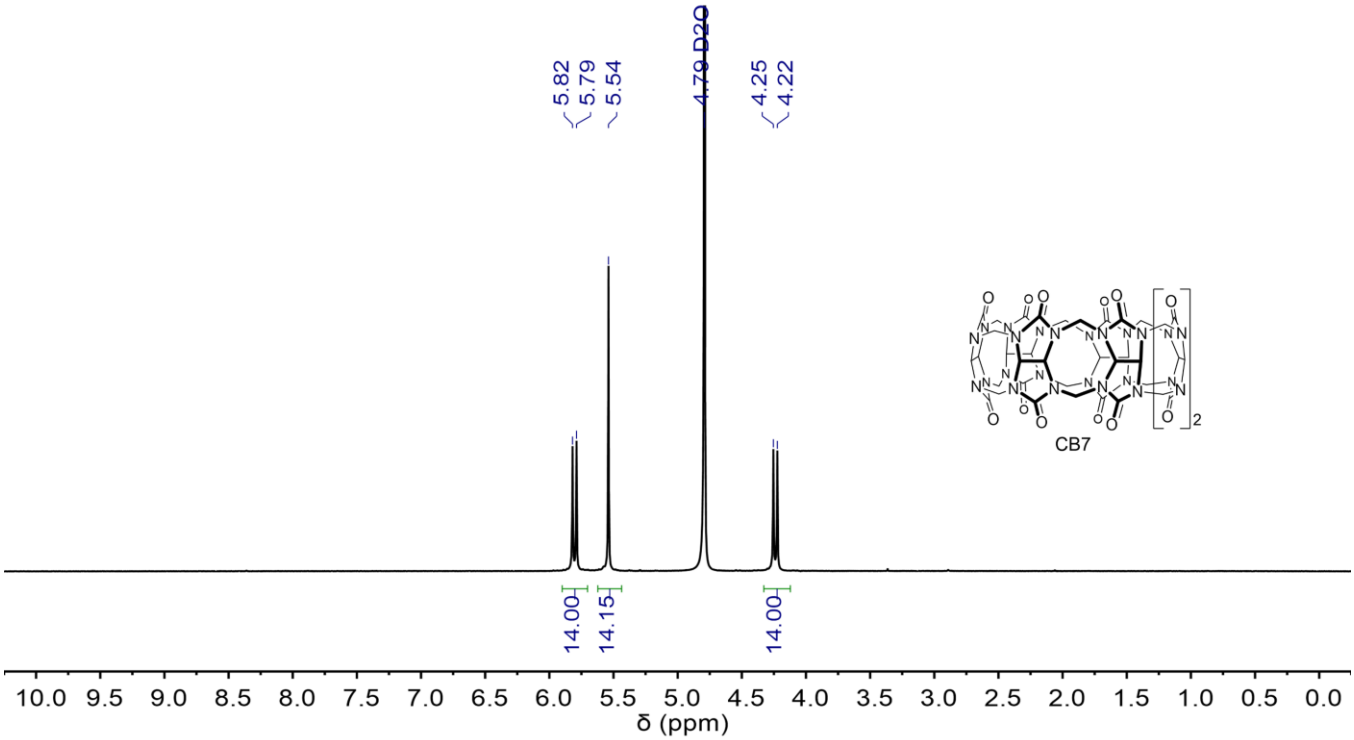

Figure S7. ^{1}H NMR spectrum of CB7 in D_2O (500 MHz, 298 K).

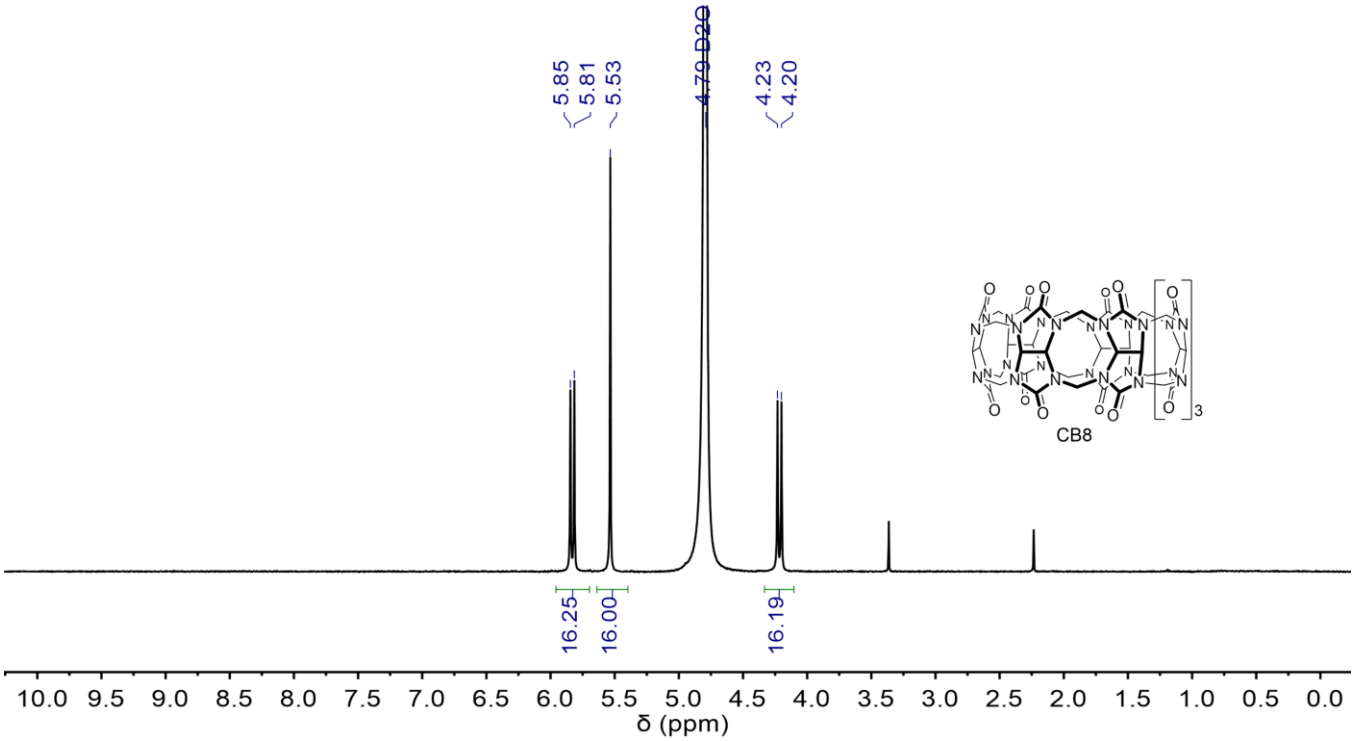

Figure S8. ^{1}H NMR spectrum of CB8 in D_2O (500 MHz, 298 K).

3. Mixed host co-assembled DimerDye•cucurbit[*n*]uril chemosensors

3.1 Cucurbit[*n*]uril into DimerDye titrations – absorbance and fluorescence

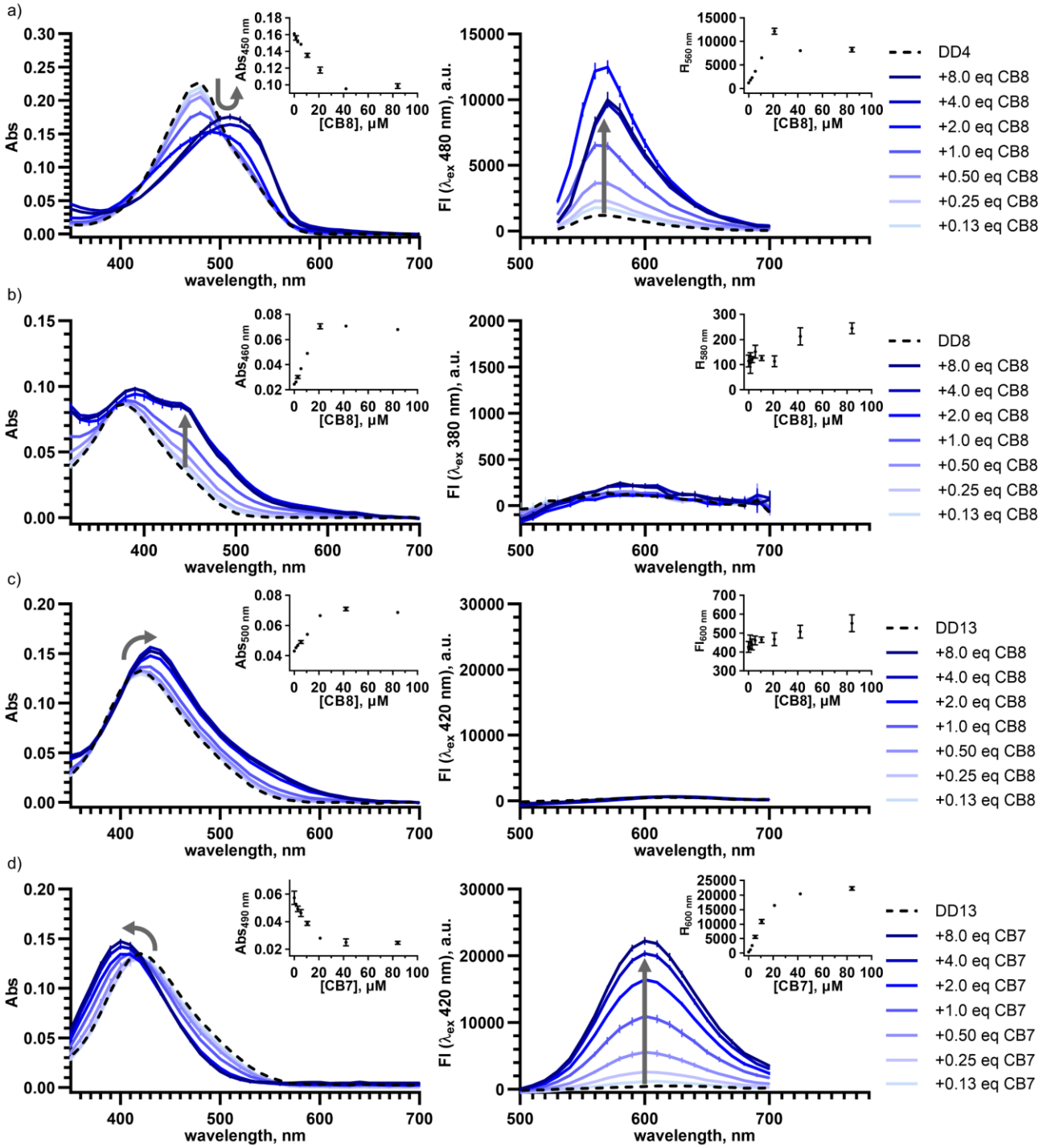

Figure S9. Titrations of cucurbit[*n*]uril into DimerDye induce red/blue shifts in absorbance and turn-on fluorescence responses. CB8 titrations into (a) DD4 (10.5 µM) (b) DD8 (10.5 µM) and (c) DD13 (10.5 µM). CB7 titration into (d) DD13 (10.5 µM). Titrations are monitored by absorbance (left) and fluorescence (right), where the darkest blue line represents the highest concentration of CB (84 µM) and the lightest blue line represents the lowest concentration of CB (1.3 µM). Traces of DimerDyes (10.5 µM) alone are shown as black dashed lines. Insets show the binding isotherms. All solutions in NaH_2PO_4/Na_2HPO_4 (10 mM, pH 7.4) in H_2O. Absorbance and fluorescence spectra are plotted as the mean of experiments done in triplicate with error bars corresponding to the standard deviation. Error bars are not visible in cases where the error is smaller than the depicted data point.

3.2 ^{1}H NMR investigation of mixed host co-assembled DD•CB chemosensor complexes

^{1}H NMR experiments were conducted to further validate DD•CB complexation interactions. Studies were limited by the solubility restraints of DD•CB complexes at concentrations required for ^{1}H NMR studies. Therefore, only mixed host complexation interactions of DD4•CB8 and DD13•CB7 were investigated by ^{1}H NMR. The turn-off fluorescence sensing mechanism of DD13•CB7 was further probed by ^{1}H NMR through the addition of a CB7 selective guest ($AdNH_3^+$). These solubility limitations prevented further experimental investigation of the size of complexes formed by dynamic light scattering (DLS) or diffusion ordered spectroscopy (DOSY).

Stock solutions of cucurbit[*n*]uril hosts (CB7 and CB8) were prepared in D_2O and concentrations were determined by titration experiments with known strong binding dyes (MDAP and BC, respectively) in H_2O.[13, 14] Stock solutions of DimerDyes (1 mM) were prepared by mass in NaH_2PO_4/Na_2HPO_4 (50 mM, pD 7.4) in D_2O. Final NMR solutions contained [DD] = 100 µM, [CB] = 100 µM in NaH_2PO_4/Na_2HPO_4 (10 mM, pD 7.4) in D_2O.

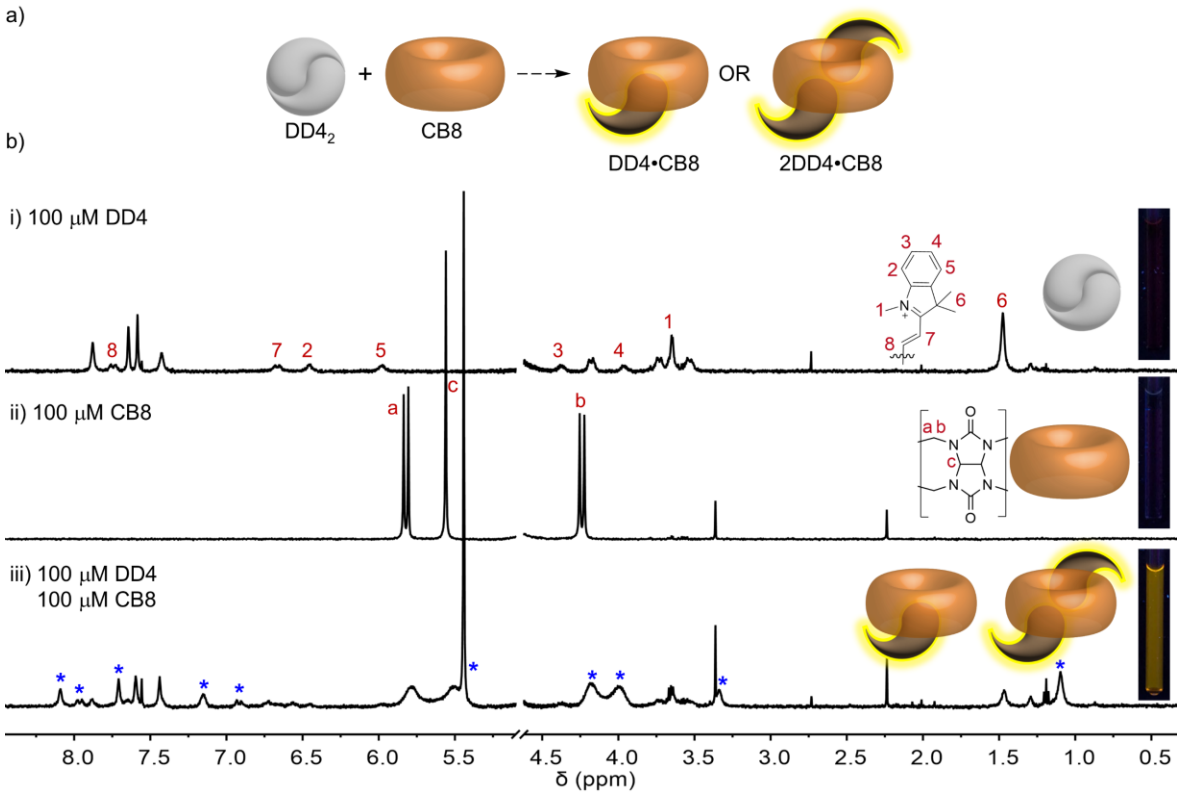

Figure S10. DD4 and CB8 form a fluorescent mixed host chemosensor. (a) Schematic of DD4•CB8 co-assembly illustrating possible binary and ternary complexes that could form in the larger CB8 cavity.[17-19] (b) ^{1}H NMR of i) DD4 (100 µM). Upfield-shifted aromatic peaks in fast exchange and non-fluorescent appearance support the existence of the homodimer $DD4_2$ in aqueous solution. ii) CB8 (100 µM). iii) DD4 (100 µM) and CB8 (100 µM) combined. Blue stars illustrate the appearance of new DD4 and CB8 resonances. The presence of new upfield-shifted and broadened aromatic peaks and upfield-shifted methyl peaks indicate DD4•CB8 complexation. Fluorescent appearance of the NMR tube further supports the disassembly of the homodimer $DD4_2$. NMR tube irradiated with a hand-held UV lamp (λ_{ex} = 356±20 nm). All samples in NaH_2PO_4/Na_2HPO_4 (10 mM, pD 7.4) in D_2O (500 MHz, 298 K).

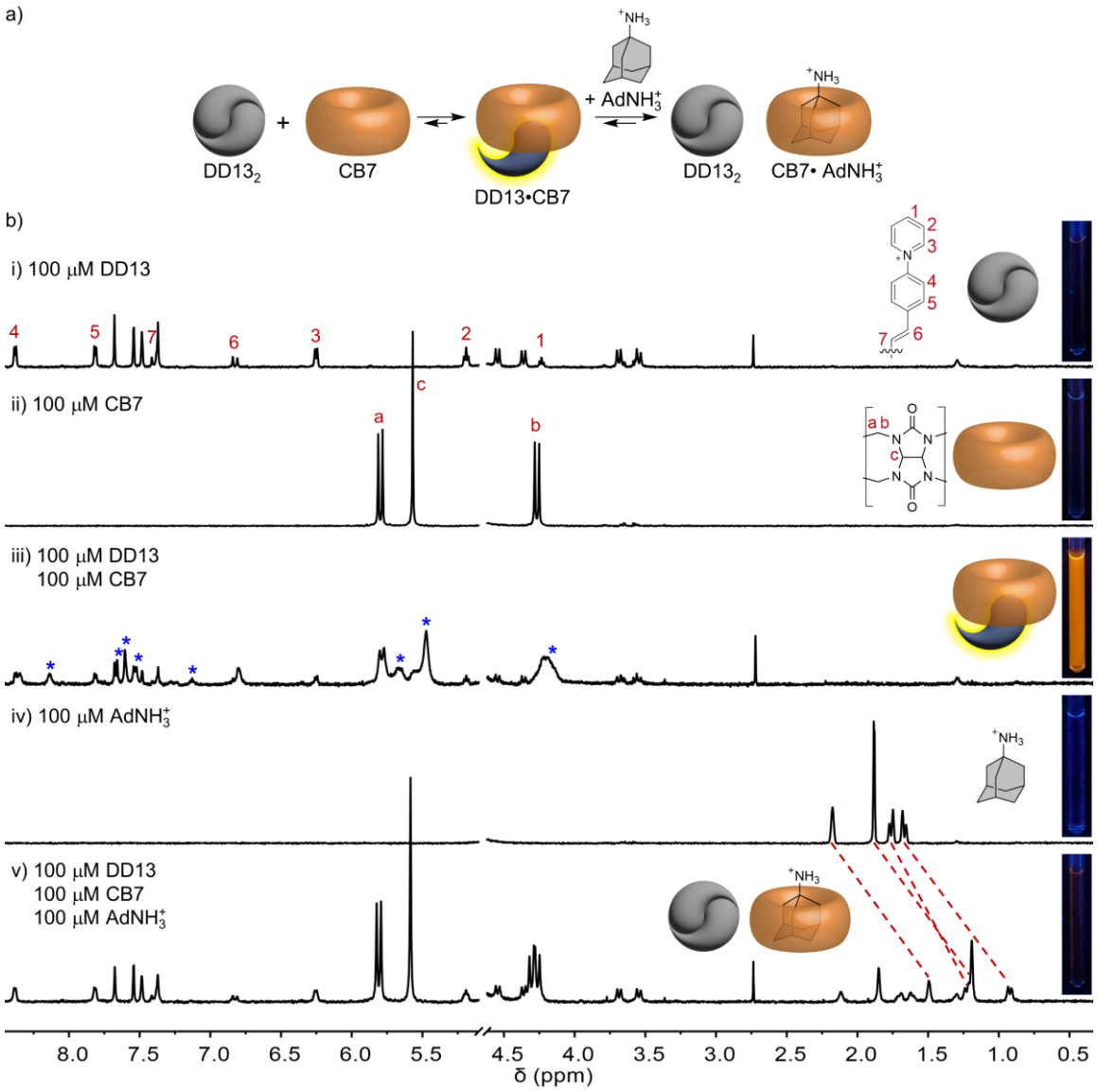

Figure S11. DD13•CB7 complex functions as a turn-off mixed host chemosensor for strong binding guests of CB7. (a) Schematic of DD13•CB7 formation and turn-off sensing mechanism upon analyte addition. (b) ^{1}H NMR of i) DD13 (100 μM) shows upfield-shifted aromatic peaks in fast exchange. Non-fluorescent appearance of the NMR tube supports the existence of homodimer DD13$_2$ in aqueous solution. ii) CB7 (100 μM). iii) DD13 (100 μM) and CB7 (100 μM) combined. Blue stars illustrate the appearance of new DD13 and CB7 resonances. The presence of new upfield-shifted and broadened aromatic peaks indicate DD4•CB8 complexation. The fluorescent appearance of the NMR tube further supports the disassembly of the homodimer DD13$_2$. iv) AdNH$_3^+$ (100 μM). v) DD13 (100 μM), CB7 (100 μM) and AdNH$_3^+$ (100 μM) combined. Upfield-shifted AdNH$_3^+$ peaks (red dashed lines) and the return of homodimer DD13$_2$ peaks indicate a CB7•AdNH$_3^+$ assembly forms. The non-fluorescent appearance of the NMR tube further supports the reformation of the homodimer DD13$_2$. NMR tube irradiated with a hand-held UV lamp (λ_{ex} 356±20 nm). All samples in NaH_2PO_4/Na_2HPO_4 (10 mM, pD 7.4) in D_2O (500 MHz, 298 K).

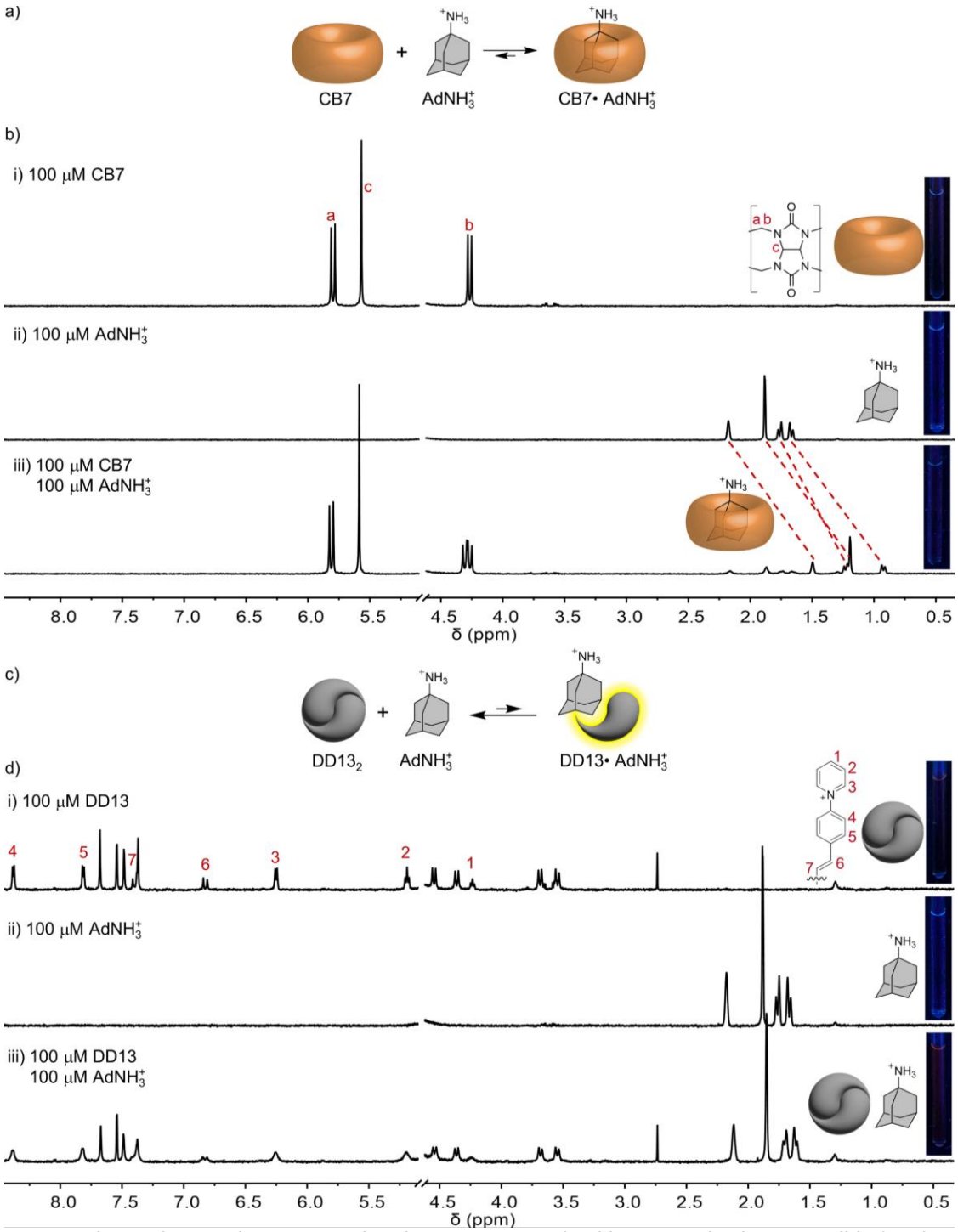

Figure S12. Control experiments demonstrate that the DD13•CB7 mixed host complex is responsible for observed sensing responses. (a) Schematic illustrating CB7•$AdNH_3^+$ favored complexation. (b) ^{1}H NMR of i) CB7 (100 μM) ii) $AdNH_3^+$ (100 μM) and iii) CB7 (100 μM) combined with $AdNH_3^+$ (100 μM). Complexation of $AdNH_3^+$ is observed by upfield-shifted resonances in slow exchange, shown as red dashed lines. All NMR tubes are non-fluorescent in appearance as CB7 and $AdNH_3^+$ are spectroscopically silent. (c) Schematic illustrating the homodimer $DD13_2$ is favored over DD13•$AdNH_3^+$ complexation. (d) ^{1}H NMR of i) DD13 (100 μM), upfield-shifted aromatic peaks in fast exchange and non-fluorescent appearance supports the existence of homodimer $DD13_2$ in aqueous solution. ii) $AdNH_3^+$ (100 μM). iii) DD13 (100 μM) and $AdNH_3^+$ (100 μM) combined. Minimal shifts observed in $AdNH_3^+$ and $DD13_2$ resonances indicate little disruption of the $DD13_2$ homodimer. The non-fluorescent appearance of the NMR tube further supports the presence of $DD13_2$ homodimer. NMR tube irradiated with a hand-held UV lamp (λ_{ex} = 356±20 nm). All samples in NaH_2PO_4/Na_2HPO_4 (10 mM, pD 7.4) in D_2O (500 MHz, 298 K).

3.3 Molecular modeling of DD13•CB7 co-assembly

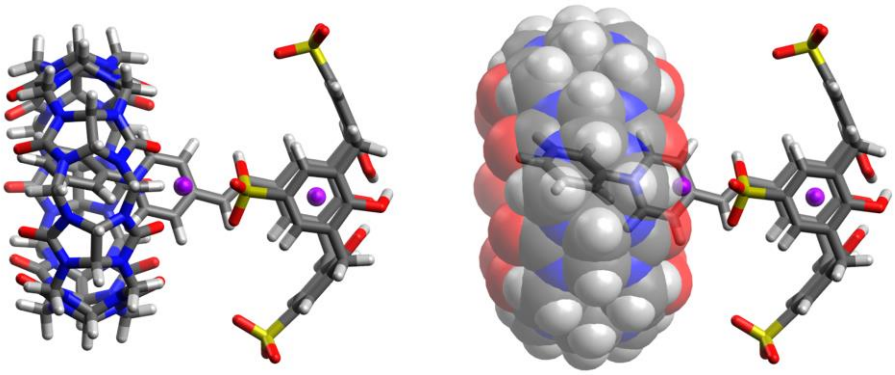

Figure S13. Molecular modeling using DFT (RWB97X-D/6-31G(D)) was performed with Spartan to illustrate a potential 1:1 binding geometry between DD13 and CB7. To partially counterbalance the overall charge of the complex, two sodium ions were strategically placed: one within the DD13 cavity, which is recognized for its Na+ binding capability, and another adjacent to the CB7 portals, known for their cation-binding affinity.[20] It is important to note that, in reality, a variety of conformers likely exist, differing in both the number and positions of bound counterions. Therefore, this molecular model should be viewed as a visual representation intended to provide insight into possible binding configurations, rather than a definitive structural depiction.

4. Identifying illicit drugs and adulterants

Discriminant analysis experiments of illicit drugs and adulterants were conducted in NUNC black-walled optical bottom 384-well plates, with 70 µL final well volumes. Final solutions contained [DD] = 10.5 µM, [CB] = 21 µM, and [drug] = 105 µM in NaH_2PO_4/Na_2HPO_4 (8.4 mM, pH 7.4) in H_2O with 2% MeOH. Mixed host chemosensor combinations of DD4•CB8, DD8•CB8, DD13•CB8, and DD13•CB7 were tested for their responses to each individual illicit drug and adulterant. Absorbance and emission wavelengths were selected based on preliminary experimental results, using excitation wavelengths at the maxima of each DimerDye (DD4 λ_{ex} = 480 nm, DD8 λ_{ex} = 380 nm and DD13 λ_{ex} = 420 nm) (Table S1). Cannabinoid sensing of DimerDyes alone was also tested using the same selected absorbance and fluorescence wavelengths (Table S2), this was done to validate the improved differentiation ability of the array of mixed host chemosensors. Absorbance and fluorescence end-point measurements of each DD•CB•drug combination were collected in 12 replicates, along with 2 solvent blank measurements. The raw data was pre-processed by subtracting the solvent blank from each DD•CB•drug measurement, then the two highest and two lowest data values were systematically excluded. Absorbance and fluorescence wavelengths that provided discrimination of drugs and adulterants were selected for PCA, while aiming to minimize the number of observations. PCA correlation plots with confidence ellipses (95%) and loading vectors were plotted on sample sets of 8 replicates using OriginPro 2022b Principal Component Analysis App (Version: 1.50, File Name: PCAC.opx).

Table S1. Mixed host chemosensor wavelengths used in PCA analysis for the identification of drugs and adulterants.

Mixed host chemosensor	Absorbance (nm)	Fluorescence (λ_{ex} (nm), λ_{em} (nm))
DD4•CB8	480	480, 570 480, 600
DD8•CB8	440	380, 570
DD13•CB8	400 430	420, 600
DD13•CB7	400 430	420, 600

Table S2. DimerDye chemosensor wavelengths used in PCA analysis for the identification of cannabinoids.

DimerDye	Absorbance (nm)	Fluorescence (λ_{ex} (nm), λ_{em} (nm))
DD4	480	480, 570 480, 600
DD8	440	380, 570
DD13	400 430	420, 600

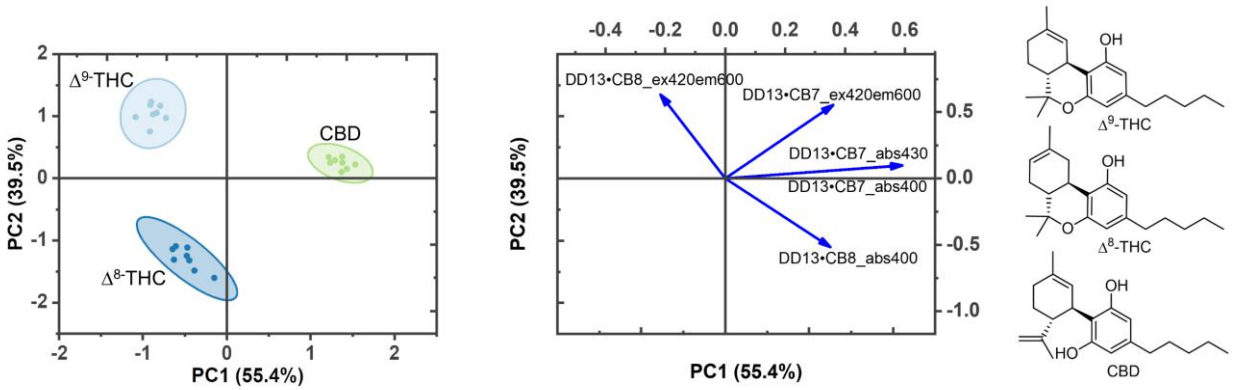

Figure S14. An array of mixed host chemosensors differentiates structurally similar neutral cannabinoids. Sensor array includes absorbance and fluorescence responses of mixed host chemosensors DD13•CB7 and DD13•CB8. PCA (correlation) score plot shows each sample set (n = 8) enclosed by 95% confidence ellipses with the respective loading plot of absorbance and fluorescence observations shown as blue arrows. Chemical structures are represented in the expected protonation forms under sensing conditions of pH 7.4. Samples contain [DD] = 10.5 µM, [CB] = 21 µM and [drug] = 105 µM. All samples are in NaH_2PO_4/Na_2HPO_4 (8.4 mM, pH 7.4) in H_2O with 2% MeOH.

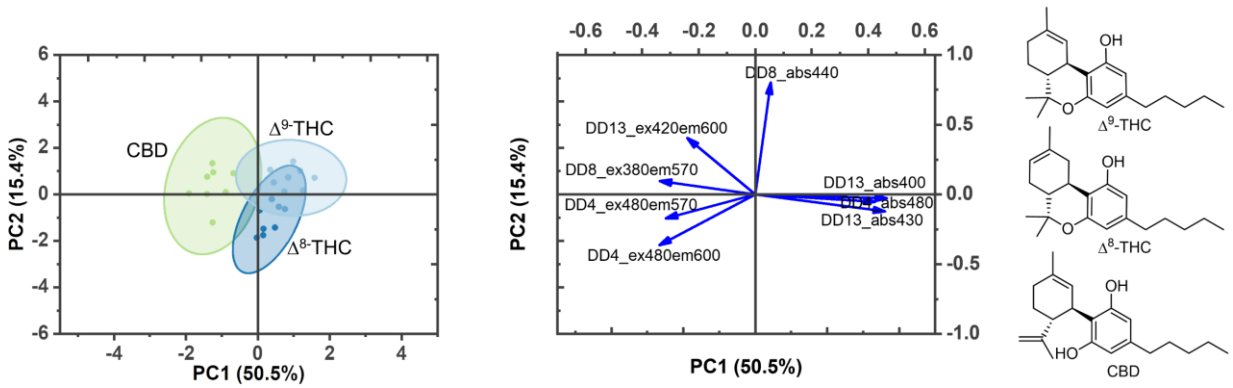

Figure S15. An array of DimerDye chemosensors does not differentiate structurally similar neutral cannabinoids. Sensor array includes absorbance and fluorescence responses of DD4, DD8, and DD13. PCA (correlation) score plot shows each sample set (n = 8) enclosed by 95% confidence ellipses with the respective loading plot of absorbance and fluorescence observations shown as blue arrows. Chemical structures are represented in the expected protonation forms under sensing conditions of pH 7.4. Samples contain [DD] = 10.5 µM and [drug] = 105 µM. All samples are in NaH_2PO_4/Na_2HPO_4 (8.4 mM, pH 7.4) in H_2O with 2% MeOH.

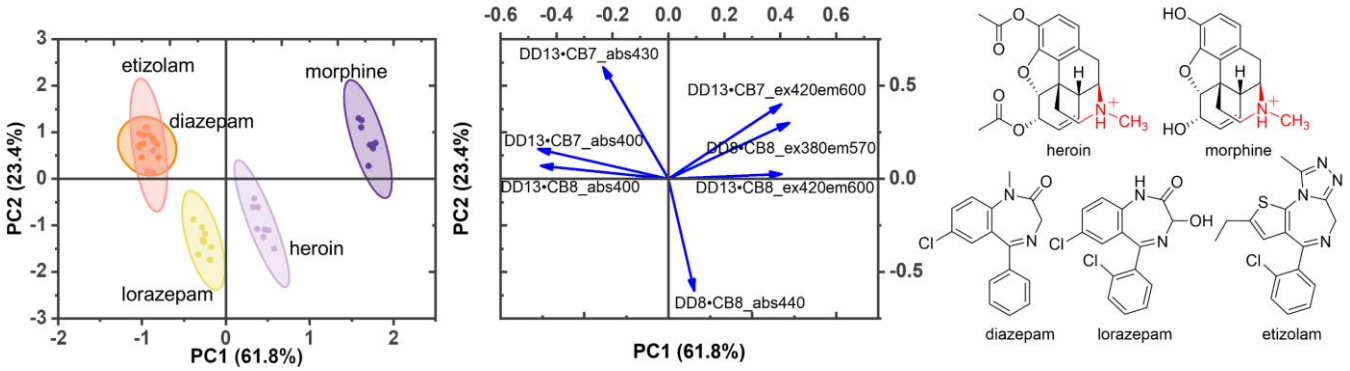

Figure S16. An array of mixed host chemosensors shows the differentiation of Central Nervous System (CNS) depressant cationic opiates and neutral benzodiazepine analogs. Sensor array includes absorbance and fluorescence responses of mixed host chemosensors DD8•CB8, DD13•CB8, and DD13•CB7. PCA (correlation) score plot shows each sample set (n = 8) enclosed by 95% confidence ellipses with the respective loading plot of absorbance and fluorescence observations shown as blue arrows. Chemical structures are represented in the expected protonation forms under sensing conditions of pH 7.4. Samples contain [DD] = 10.5 µM, [CB] = 21 µM, [drug] = 105 µM. All samples are in NaH_2PO_4/Na_2HPO_4 (8.4 mM, pH 7.4) in H_2O with 2% MeOH.

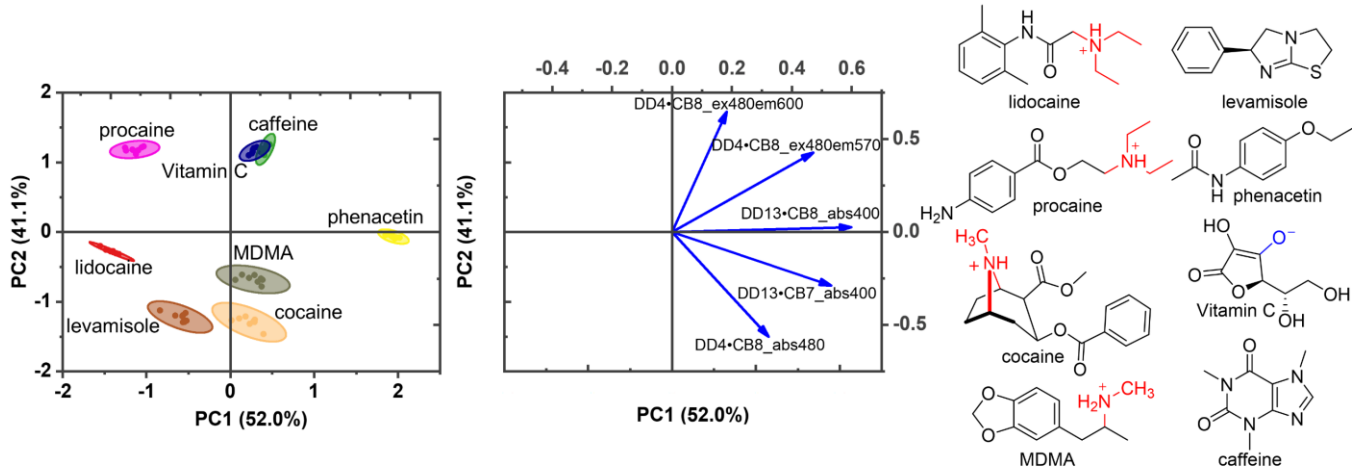

Figure S17. An array of mixed host chemosensors discriminates anesthetics and amphetamine from common adulterants. Sensor array includes absorbance and fluorescence responses of mixed host chemosensors DD4•CB8, DD13•CB8, and DD13•CB7. PCA (correlation) score plot shows each sample set (n = 8) enclosed by 95% confidence ellipses with the respective loading plot of absorbance and fluorescence observations shown as blue arrows. Chemical structures are represented in the expected protonation forms under sensing conditions of pH 7.4. Samples contain [DD] = 10.5 µM, [CB] = 21 µM and [drug] = 105 µM. All samples are in NaH_2PO_4/Na_2HPO_4 (8.4 mM, pH 7.4) in H_2O with 2% MeOH.

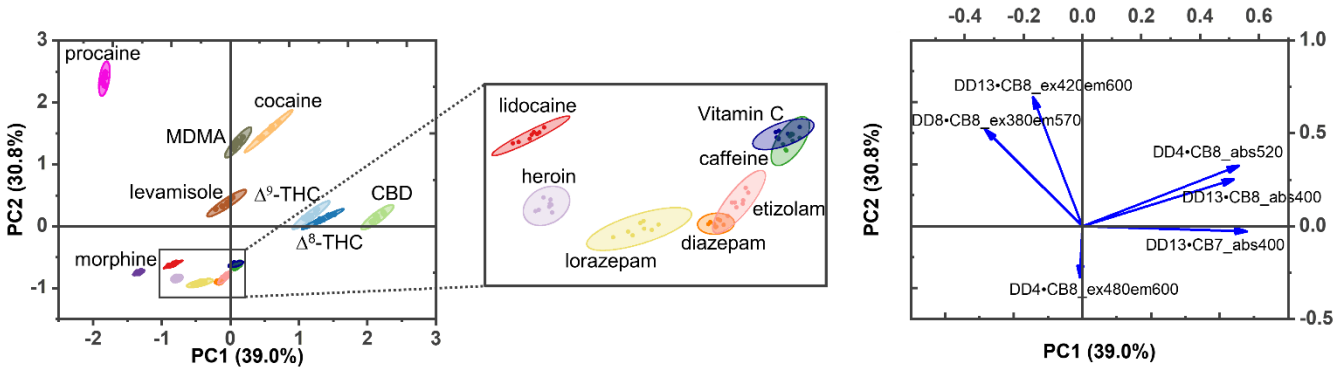

Figure S18. All drug and adulterant differentiation from an array of mixed host chemosensors. Sensor array includes absorbance and fluorescence responses from mixed host chemosensors DD4•CB8, DD8•CB8, DD13•CB8, and DD13•CB7. PCA (correlation) score plot shows each sample set (n = 8) enclosed by 95% confidence ellipses with the respective loading plot of absorbance and fluorescence observations shown as blue arrows. Samples contain [DD] = 10.5 µM, [CB] = 21 µM, [drug] = 105 µM. All samples are in NaH_2PO_4/Na_2HPO_4 (8.4 mM, pH 7.4) in H_2O with 2% MeOH.

5. Identifying multi-component street drug samples

Discriminant analysis experiments of multi-component street drug samples were conducted in NUNC black-walled optical bottom 384-well plates, with 50 µL final well volumes. Final solutions contained [DD] = 10.5 µM, [CB] = 21 µM, [street drug sample] = 0.03 mg/mL in NaH_2PO_4/Na_2HPO_4 (8.4 mM, pH 7.4) in H_2O with 2% MeOH. A blank of each multi-component street drug sample was measured to ensure no signal overlap in the DimerDye regions. Full absorbance and fluorescence spectral scans of each combination were collected in 12 replicates, along with 2 solvent blank measurements. Full spectral scans were collected to cover any binding induced changes in λ_{max} occurring in the multi-component mixtures (Figure S19 and S20). Excitation wavelengths were selected at the maxima of each DimerDye (DD4 λ_{ex} = 480 nm, DD8 λ_{ex} = 380 nm, DD13 λ_{ex} = 420 nm). A second set of absorbance spectral scans was taken after the experiment was completed and compared to the measurements from the start of the experiment, this was done to ensure there were no changes in the spectra throughout the course of experimental measurements and a steady equilibrium was reached within the multi-component mixtures. Collected raw data was preprocessed by subtracting a buffer blank from absorbance and fluorescence readings. Absorbance and fluorescence wavelengths from the mixed host chemosensors that provided different responses to the multi-component street drug samples were selected for PCA discrimination, while aiming to use a minimal number of observations (Table S3). DimerDye chemosensors alone were also tested using the same selected absorbance and fluorescence wavelengths (Table S4) as a direct comparison of the DimerDye sensor array (Figure S22) to the array of DD•CB mixed host chemosensors (Figure S21). PCA correlation plots with confidence ellipses (95%) and loading vectors were plotted on sample sets of 8 replicates using OriginPro 2022b Principal Component Analysis App (Version: 1.50, File Name: PCAC.opx).

Table S3. Mixed host chemosensor wavelengths used in PCA analysis for the identification of multi-component street drug samples.

Mixed host chemosensor	Absorbance (nm)	Fluorescence ($\lambda_{ex.}$ nm, $\lambda_{em.}$ nm)
DD4•CB8	-	480, 570 480, 580
DD8•CB8	-	380, 580
DD13•CB8	430	420, 600
DD13•CB7	400	420, 600

Table S4. DimerDye chemosensor wavelengths used in PCA analysis for the identification of multi-component street drug samples.

DimerDye	Absorbance (nm)	Fluorescence ($\lambda_{ex.}$ nm, $\lambda_{em.}$ nm)
DD4	-	480, 570 480, 580
DD8	-	380, 580
DD13	400 430	420, 600

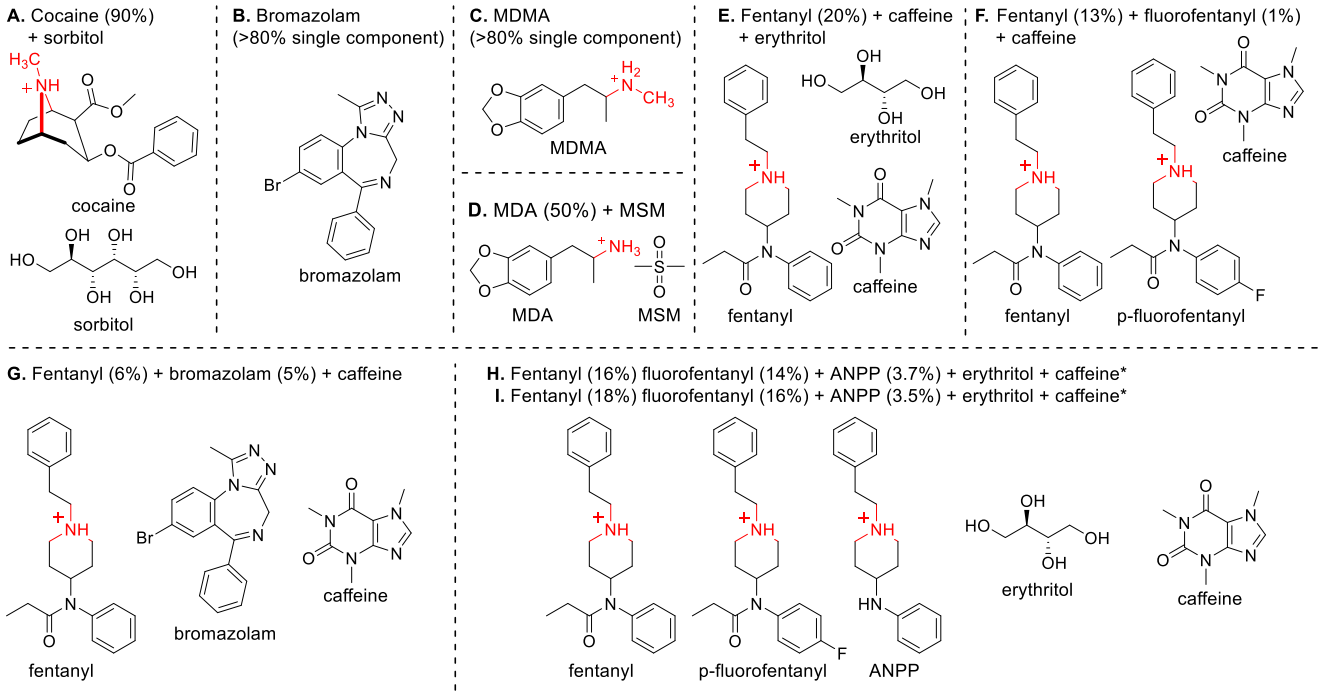

Figure S19. Composition and chemical structures of the multi-component street drug samples acquired through Substance, the Vancouver Island Drug Checking Project, located in Victoria, British Columbia, Canada.[5] *Samples H and I were provided by two different people reporting the same drug from the same batch and supplier. All chemical structures are represented in the expected protonation forms under sensing conditions of pH 7.4.

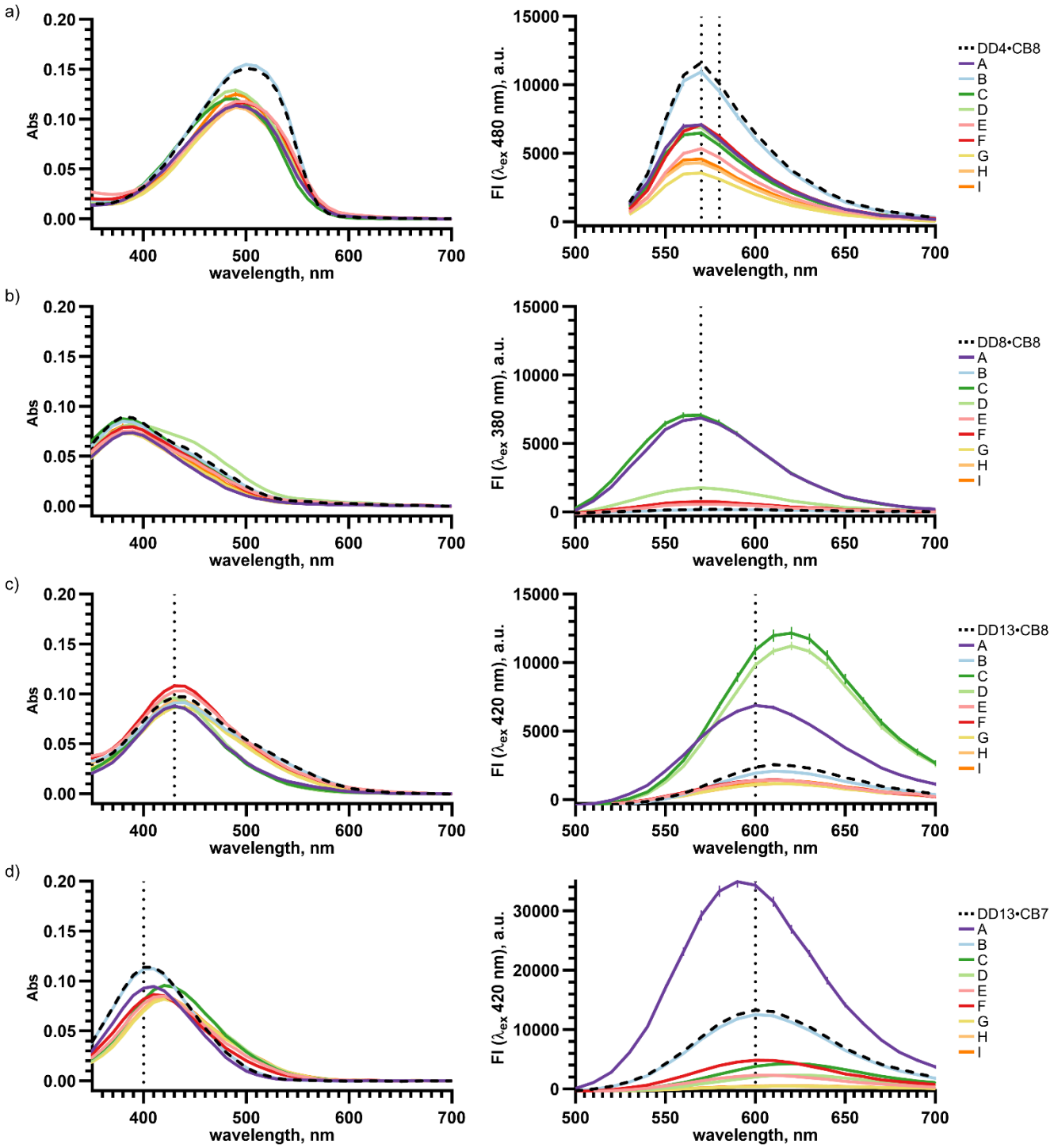

Figure S20. Mixed host chemosensor absorbance and fluorescence responses to multi-component street drug samples. Absorbance responses (left) and fluorescence responses (right) of mixed host chemosensors (a) DD4•CB8, (b) DD8•CB8, (c) DD13•CB8 and (d) DD13•CB7 to multi-component street drug samples A-I (Table 1, Figure S18). The dotted lines in the spectra represent the selected wavelengths used in PCA analysis. Samples contain [DD] = 10.5 μM, [CB] = 21 μM, and [street drug sample] = 0.03 mg/mL. All samples are in NaH_2PO_4/Na_2HPO_4 (8.4 mM, pH 7.4) in H_2O with 2% MeOH.

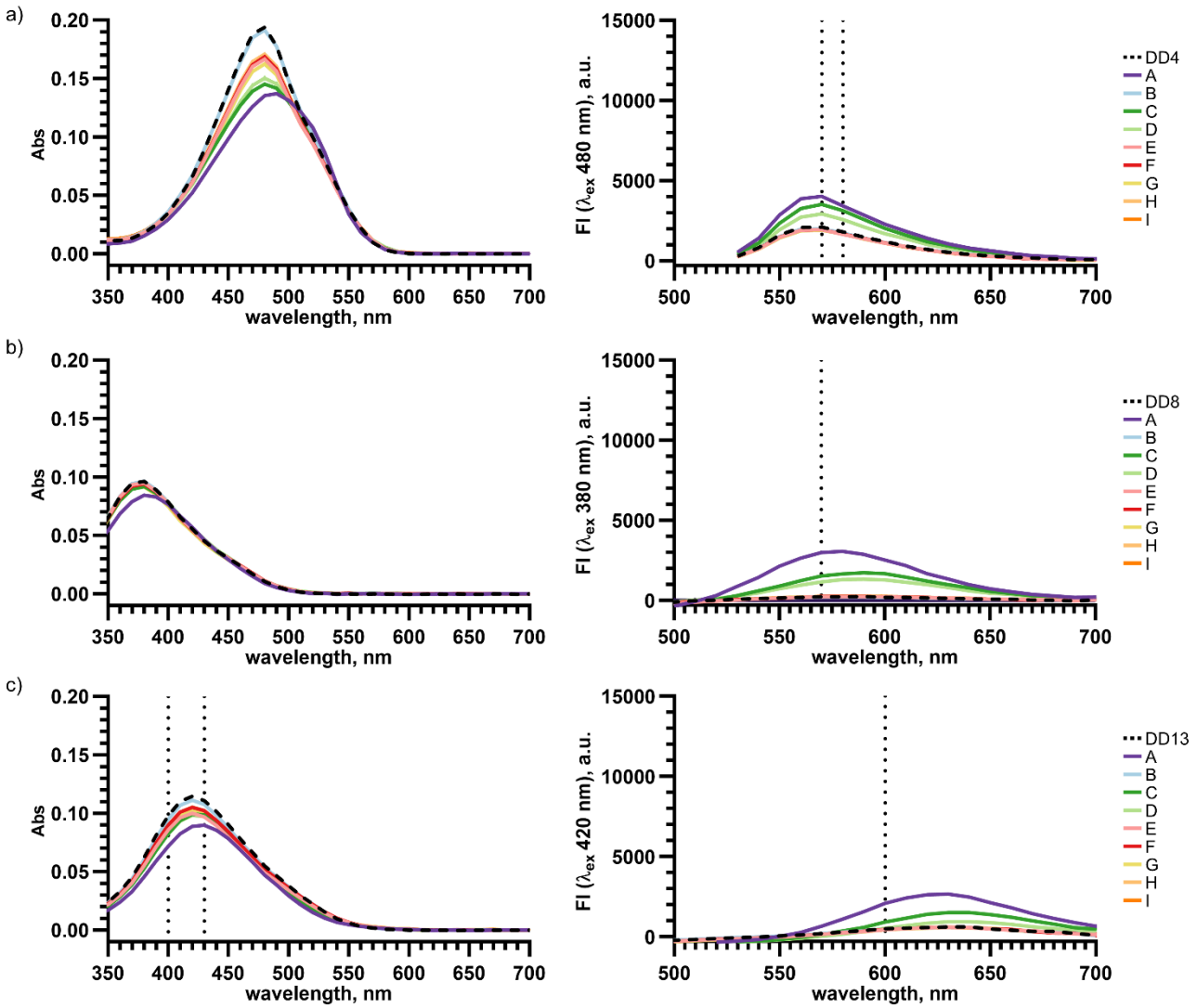

Figure S21. DimerDye absorbance and fluorescence responses to multi-component street drug samples. Absorbance responses (left) and fluorescence responses (right) of DimerDyes (a) DD4 (b) DD8 and (c) DD13 to multi-component street drug samples A-I (Table 1, Figure S18). The dotted lines in the spectra represent the selected wavelengths used in PCA analysis. Samples contain [DD] = 10.5 μM and [street drug sample] = 0.03 mg/mL. All samples are in NaH_2PO_4/Na_2HPO_4 (8.4 mM, pH 7.4) in H_2O with 2% MeOH.

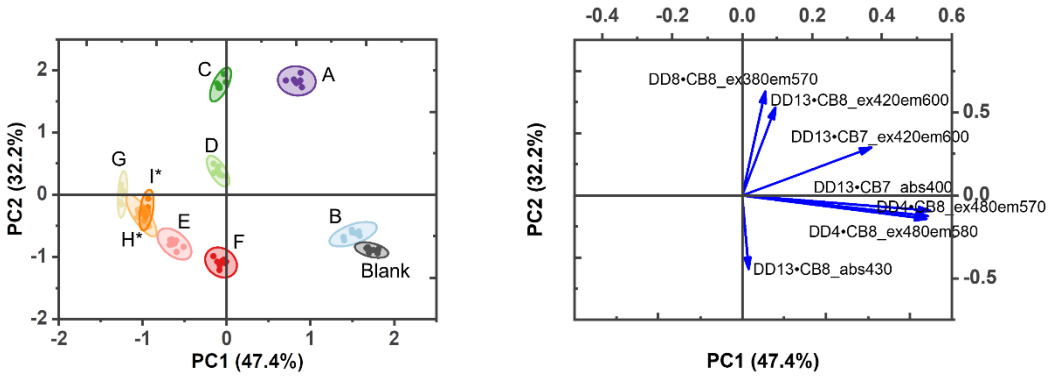

Figure S22. An array of mixed host chemosensors differentiates multi-component street drug samples. Sensor array includes absorbance and fluorescence responses from mixed host chemosensors DD4•CB8, DD8•CB8, DD13•CB8, and DD13•CB7. PCA (correlation) score plot shows each sample set (n = 8) enclosed by 95% confidence ellipses with the respective loading plot of absorbance and fluorescence observations shown as blue arrows. Samples contain [DD] = 10.5 µM, [CB] = 21 µM, and [street drug sample] = 0.03 mg/mL. All samples are in NaH_2PO_4/Na_2HPO_4 (8.4 mM, pH 7.4) in H_2O with 2% MeOH.

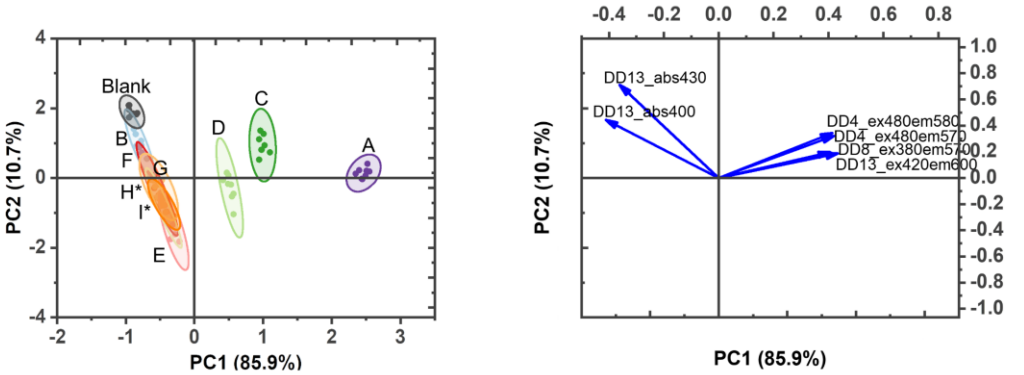

Figure S23. An array of DimerDye chemosensors does not differentiate street drug samples. PCA (correlation) score plot shows each samples set (n = 8) enclosed by 95% confidence ellipses with the respective loading plot of absorbance and fluorescence observations shown as blue arrows. Samples contain [DD] = 10.5 µM and [street drug sample] = 0.03 mg/mL. All samples are in NaH_2PO_4/Na_2HPO_4 (8.4 mM, pH 7.4) in H_2O with 2% MeOH.

References

(1) Beatty, M. A.; Selinger, A. J.; Li, Y.; Hof, F. Parallel Synthesis and Screening of Supramolecular Chemosensors that Achieve Fluorescent Turn-on Detection of Drugs in Saliva. *J. Am. Chem. Soc.* **2019**, *141*, 16763-16771. DOI: 10.1021/jacs.9b07073.
(2) Kim, J.; Jung, I.-S.; Kim, S.-Y.; Lee, E.; Kang, J.-K.; Sakamoto, S.; Yamaguchi, K.; Kim, K. New Cucurbituril Homologues: Syntheses, Isolation, Characterization, and X-ray Crystal Structures of Cucurbit[*n*]uril (n = 5, 7, and 8). *J. Am. Chem. Soc.* **2000**, *122*, 540-541. DOI: 10.1021/ja993376p.
(3) Jiao, D.; Scherman, O. A. Isolation of cucurbit[n]uril homologues with imidazolium salts in a recyclable manner. *Green Chem.* **2012**, *14*, 2445. DOI: 10.1039/c2gc35283d.
(4) Blacker, A. J.; Jazwinski, J.; Lehn, J.-M. Molecular Anion Binding and Substrate Photooxidation in Visible Light by 2,7-Diazapyrenium Cations. *Helv. Chim. Acta.* **1987**, *70*, 1-12. DOI: 10.1002/hlca.19870700102.
(5) *Substance: Vancouver Island Drug Checking Project*. https://substance.uvic.ca.
(6) Wallace, B.; Hills, R.; Rothwell, J.; Kumar, D.; Garber, I.; Van Roode, T.; Larnder, A.; Pagan, F.; Aasen, J.; Weatherston, J.; et al. Implementing an integrated multi-technology platform for drug checking: Social, scientific, and technological considerations. *Drug Test Anal.* **2021**, *13*, 734-746. DOI: 10.1002/dta.3022.
(7) Gozdzialski, L.; Hutchison, A.; Wallace, B.; Gill, C.; Hore, D. Toward Automated Infrared Spectral Analysis in Community Drug Checking. *Drug Test Anal.* **2023**. DOI: 10.1002/dta.3520.
(8) Borden, S. A.; Saatchi, A.; Vandergrift, G. W.; Palaty, J.; Lysyshyn, M.; Gill, C. G. A New Quantitative Drug Checking Technology for Harm Reduction: Pilot Study in Vancouver, Canada Using Paper Spray Mass Spectrometry. *Drug Alcohol Rev.* **2022**, *41*, 410-418. DOI: 10.1111/dar.13370.
(9) Borden, S. A.; Saatchi, A.; Krogh, E. T.; Gill, C. G. Rapid and Quantitative Determination of Fentanyls and Pharmaceuticals from Powdered Drug Samples by Paper Spray Mass Spectrometry. *Anal. Sci. Adv.* **2020**, *1*, 97-108. DOI: 10.1002/ansa.202000083.
(10) Gozdzialski, L.; Rowley, A.; Borden, S. A.; Saatchi, A.; Gill, C. G.; Wallace, B.; Hore, D. K. Rapid and Accurate Etizolam Detection Using Surface-Enhanced Raman Spectroscopy for Community Drug Checking. *Int. J. Drug Policy* **2022**, *102*, 103611. DOI: 10.1016/j.drugpo.2022.103611.
(11) *Paper Spray Mass Spectrometry Target List by Category*. https://substance.uvic.ca/paperspray.
(12) Krezel, A.; Bal, W. A Formula for Correlating pK_a Values Determined in D_2O and H_2O. *J. Inorg. Biochem.* **2004**, *98*, 161-166. DOI: 10.1016/j.jinorgbio.2003.10.001.
(13) Prabodh, A.; Bauer, D.; Kubik, S.; Rebmann, P.; Klärner, F. G.; Schrader, T.; Delarue Bizzini, L.; Mayor, M.; Biedermann, F. Chirality Sensing of Terpenes, Steroids, Amino Acids, Peptides and Drugs with Acyclic Cucurbit[*n*]urils and Molecular Tweezers. *Chem. Commun.* **2020**, *56*, 4652-4655. DOI: 10.1039/d0cc00707b.
(14) Prabodh, A.; Sinn, S.; Biedermann, F. Analyte Sensing with Unselectively Binding Synthetic Receptors: Virtues of Time-Resolved Supramolecular Assays. *Chem. Commun.* **2022**, *58*, 13947-13950. DOI: 10.1039/d2cc04831k.
(15) Swinehart, D. F. The Beer-Lambert Law. *J. Chem. Educ.* **1962**, *39*, 333. DOI: 10.1021/ed039p333.
(16) Beatty, M. A.; Borges-González, J.; Sinclair, N. J.; Pye, A. T.; Hof, F. Analyte-Driven Disassembly and Turn-On Fluorescent Sensing in Competitive Biological Media. *J. Am. Chem. Soc.* **2018**, *140*, 3500-3504. DOI: 10.1021/jacs.7b13298.
(17) Liu, J.; Lambert, H.; Zhang, Y.-W.; Lee, T.-C. Rapid Estimation of Binding Constants for Cucurbit[8]uril Ternary Complexes Using Electrochemistry. *Anal. Chem.* **2021**, *93*, 4223-4230. DOI: 10.1021/acs.analchem.0c04887.
(18) Biedermann, F.; Ross, I.; Scherman, O. A. Host–guest accelerated photodimerisation of anthracene-labeled macromolecules in water. *Polym. Chem.* **2014**, *5*. DOI: 10.1039/c4py00627e.
(19) Sayed, M.; Biedermann, F.; Uzunova, V. D.; Assaf, K. I.; Bhasikuttan, A. C.; Pal, H.; Nau, W. M.; Mohanty, J. Triple emission from p-dimethylaminobenzonitrile-cucurbit[8]uril triggers the elusive excimer emission. *Chem. Eur. J.* **2015**, *21*, 691-696. DOI: 10.1002/chem.201404902.
(20) Zhang, S.; Grimm, L.; Miskolczy, Z.; Biczók, L.; Biedermann, F.; Nau, W. M. Binding affinities of cucurbit[*n*]urils with cations. *Chem. Commun.* **2019**, *55*, 14131-14134. DOI: 10.1039/c9cc07687e.